

# Robust DOA Estimation Using Acoustic Vector Sensor Arrays with Time-varying Axial Deviation under Non-uniform Noise

Weidong Wang, Affaq Qamar, Linya Ma, Hui Li, Zhiqiang Liu, Wentao Shi, Wasiq Ali, and Sheeraz Akram

**Abstract**—To mitigate the significant degradation in direction of arrival (DOA) estimation performance caused by time-varying axial deviation (TVAD) in acoustic vector sensor (AVS) array under non-uniform noise, a two-step least squares fitting (TSLSF) technique is presented in this paper. Firstly, a model for the AVS array incorporating TVAD is established by introducing axial deviation parameters into datasets from various sub-time periods (STPs). Then, to treat the noise vectors of each channel in the AVS array as virtual sparse signals, a novel AVS array manifold matrix is formulated. After that, to estimate the TVAD matrix, sparse signals, and noise vector, two cost functions are constructed based on the principle of weighted least squares. Moreover, their analytical expressions were derived. Furthermore, to handle the effects of TVAD on DOA estimation performance over the entire observation period, the focusing technology is adopted to transform datasets with TVAD from different STPs into the desired dataset. Simulation experiments confirmed the effectiveness and resilience of the proposed method using an AVS array in conjunction with TVAD in the presence of non-uniform noise.

**Index Terms**—Acoustic vector sensor (AVS) array, direction of arrival (DOA) estimation, non-uniform noise, time-varying axial deviation (TVAD).

## I. INTRODUCTION

ACCURATELY determining the direction of arrival (DOA) for underwater targets is a crucial aspect in passive sonar detection and localization. In practical engineering applications, the traditional acoustic pressure

Manuscript received February 4, 2025; revised July 7, 2025; approved for publication by Gaillot, Davy, Division 2 Editor, September 8, 2025.

This work was supported and funded by the Deanship of Scientific Research at Imam Mohammad Ibn Saud Islamic University (IMSIU) (grant number IMSIU-DDRSP2503).

W. Wang, L. Ma, and H. Li are with the School of Physics and Electronic Information Engineering, Henan Polytechnic University, Jiaozuo 454000, China, email: wwd@hpu.edu.cn, mly@home.edu.cn, li20022004@hpu.edu.cn.

A. Qamar is with Department of Electrical Engineering, College of Engineering, Imam Mohammad Ibn Saud Islamic University (IMSIU) Riyadh, 11564, Kingdom of Saudi Arabia, email: aaqamar@imamu.edu.sa.

Z. Liu is with School of Software, Henan Polytechnic University, Jiaozuo, 454003, China, email: liuzq@hpu.edu.cn.

W. Shi is with Ocean Institute of Northwestern Polytechnical University, Taiyang, 215400, China, email: swt@nwpu.edu.cn.

W. Ali is with the College of Underwater Acoustic Engineering, Harbin Engineering University, Harbin, 150001, China, email: wasiqali@hrbeu.edu.cn.

S. Akram is with Information Systems Department, College of Computer and Information Sciences, Imam Mohammad Ibn Saud Islamic University (IMSIU) Riyadh, 11564, Kingdom of Saudi Arabia, email: sakram@imamu.edu.sa.

W. Ali is the corresponding author.

Digital Object Identifier: 10.23919/JCN.2025.000071

sensor (APS) array being used for estimating the DOA of underwater sources often encounters challenges, such as enhancing the DOA resolution and estimation accuracy for low-frequency signals, which often necessitates increasing the aperture of the APS array, as well as the inability to distinguish the left/right ambiguity. Given the capability of a single acoustic vector sensor (AVS) to concurrently measure both sound pressure and acoustic particle velocity (APV) information within the sound field, the utilization of AVS arrays offers a comprehensive approach to address the aforementioned challenges [1], [2]. Therefore, the AVS arrays, which offer numerous advantages over APS arrays that are only capable of acquiring sound pressure information, have extremely important application in various fields such as marine environmental monitoring [3], underwater target detection [4], underwater communication [5], as well as marine renewable energy [6]–[8].

The DOA estimation techniques including ESPRIT [9], MUSIC [10], and sparse representation methods, such as  $\ell_1$ -norm based singular value decomposition (L1SVD) method [11], iteration adaptive approach (IAA) [12], and their improved algorithms [13], [14] are originally devised for the APS array. These methods have been successfully applied through AVS array [15]–[20]. The exceptional effectiveness of DOA estimation methods such as ESPRIT, MUSIC, and sparse representation techniques significantly relies on the presumed condition that the noise captured by the array displays a diagonal covariance matrix with identical diagonal components, indicating uniform noise across all array elements. However, in practical engineering application scenarios, as reported in [21], [22], the underwater AVS primarily encounter ambient noise as the dominant noise source, in which case, the noise powers received by the APS and APV segments of the AVS array are unequal. Specifically, the APV component, due to its directional characteristics, possesses the capability to filter out certain noise components, resulting in a lower noise power compared to the APS components. In this scenario, although the noise covariance matrix of the AVS array continues to be diagonal, the coefficients of the APS element along the diagonal vary from the coefficients of the APV element for each AVS within the array. Noting that each AVS in the array exhibits equal noise variance in their APS components and also equal noise variance in their APV components in the presence of ambient noise. However, each channel in the array may encounter different levels of noise variance due to the inherent

Creative Commons Attribution-NonCommercial (CC BY-NC).

This is an Open Access article distributed under the terms of Creative Commons Attribution Non-Commercial License (<http://creativecommons.org/licenses/by-nc/3.0/>) which permits unrestricted non-commercial use, distribution, and reproduction in any medium, provided that the original work is properly cited.

imperfect channel response of each AVS. This form of noise is classified as non-uniform noise. It should be noted that the ambient noise aligns with uniform noise when the APS and APV components of each AVS in the array have the same noise variance in the ambient noise.

Numerous efforts in the past decade have yielded robust algorithms to address the challenge of DOA estimation in non-uniform noise environments. These algorithms are capable of accurately estimating the DOA despite the varying levels of noise present across different channels [23]–[27]. Although the above methods can be applied to AVS arrays to solve the problem of reduced DOA prediction efficiency under non-uniform noise conditions, the aforementioned methods frequently encounter challenges in iterative processes and nonlinear optimization, leading to a large amount of computational overhead. To address this limitation, an augmented subspace MUSIC (ASMUSIC) algorithm was introduced in [21]. ANEMUSIC, an enhanced MUSIC DOA estimation approach with asymptotically ambient noise elimination, was derived by leveraging the actual and imaginary components of the autocorrelation and cross-correlation of the ambient noise [22]. Furthermore, M. Wang et al. [28] presents a coordinate descent method, rooted in factor analysis tailored for anisotropic noise scenarios, intended to alleviate the impact of uneven noise. It is important to acknowledge the works in [21], [22], [28], which primarily focus on addressing unequal noise power within individual APS and APV sensors of a single AVS system, overlooking the potential for unequal noise power across sensors, belonging to different AVS units within the array. As a result, the APS and APV sensors of different AVSs may experience unequal noise power when AVS units exhibit different response, drastically reduces the DOA estimation accuracy of various approaches.

A basic premise of the above method is that during the data acquisition process, all APV axes are aligned in the same direction, and the AVS array is stable. However, in complex underwater environments, the inherent directionality of APV components, coupled with environmental factors such as buoyancy and ocean currents, may cause them to deviate from the initial reference orientation. In other words, if all the APV axes in the AVS array do not point in the same direction, we refer to this situation as axial deviation in the AVS array. To mitigate the challenges, an alternating iterative adaptive strategy was introduced in [19], aiming to handle its impact on DOA estimation. Furthermore, W. Shi [29] presented a sparse alternating iterative minimization technique, which reconstructs the axial deviation matrix leveraging its distribution properties, enhancing DOA estimation accuracy. Additionally, S. Shi [30] developed eigenstructure-based estimation algorithms utilizing both the APV and APS analytics to bolster DOA estimation performance for circular AVS arrays under axial deviation. In reality, considerable research has been conducted in [19], [29], [30] to address this challenge. However, these methods have predominantly focused their investigations under the assumption of a invariant axial deviation throughout the entire duration of data collection by the AVS arrays. In real-world scenarios, the APV axis of AVS arrays is prone to temporal variations influenced by the marine

environment, leading to time-varying axial deviation (TVAD) in the collected data throughout the observation period. To address the significant impacts of these deviations on DOA estimation, the covariance matrix focusing fitting (CMFF) technique was proposed as outlined in [31]. However, this method only focuses on tackling the problem of TVAD in the AVS array while overlooking the possible impact of non-uniform noise on the precision of DOA estimation.

In conclusion, the aforementioned techniques can only handle situations with inconsistent noise or invariant axial deviation or TVAD. Yet, the DOA detection abilities of AVS arrays in practical engineering applications, where inconsistent noise and TVAD coexist, have received little attention. To bridge this gap, this paper introduces a two-step least squares fitting (TSLSF) technique, which robustly estimates DOA and effectively counter the coexistence of these challenges. The following is a summary of the primary findings of this study:

- A novel DOA estimation framework is formulated for AVS array with TVAD, in which an enhanced data model is developed by integrating deviation parameters into STPs. The proposed framework employs a weighted least squares approach to improve estimation accuracy under structural perturbations.
- A robust optimization strategy is introduced to address the uncertainty induced by axial deviations, where a majorization-minimization algorithm is employed to convert the non-convex estimation problem into a uniform and tractable form. Furthermore, the application of spatial focusing techniques across STPs significantly mitigates the degradation of DOA performance caused by AVS array deviations.
- A sparsity-driven signal reconstruction model is developed for the AVS array, where the noise vector is exploited as a sparse candidate to enhance resolution. By reformulating the interference-plus-noise covariance matrix, the proposed algorithm accurately identifies source directions through peak detection over the reconstructed sparse signals.
- The proposed method demonstrates superior robustness and accuracy in challenging scenarios, particularly in environments with non-uniform noise and uncertain array configurations, as validated through extensive simulations and comparative evaluations with benchmark algorithms.

**Notations:** The pseudo-inverse, conjugate transpose, and transpose of the matrix  $\mathbf{B}$  are shown as  $\mathbf{B}^\dagger$ ,  $\mathbf{B}^H$ , and  $\mathbf{B}^T$ , respectively. The notation  $(\cdot)^{(j)}$  with a superscript  $j$  signifies the  $j$ th iteration of the enclosed operation.  $\text{Trace}\{\cdot\}$  computes the trace of a matrix. The Kronecker product's operation is represented by the symbol  $\otimes$ . The symbols  $\text{diag}(\cdot)$  and  $\text{blkdiag}(\cdot)$  are used for the operations of matrix diagonalization and block diagonalization, respectively. The Frobenius norm of a matrix is represented by  $\|\cdot\|_F$ .  $\mathbf{E}_M$  designates the identity matrix of dimension  $M \times M$ .

## II. PROBLEM DESCRIPTION

### A. The Ideal AVS Array Model

An underwater uniform linear array with  $M$  AVS elements arranged at a spacing of  $d$  is considered, where the AVS

elements represent  $u_x$  and  $u_y$  orthogonal APV elements, as illustrated in Fig. 1(a), and if the array is under the influence of  $K$  narrowband far-field source signals arriving from directions  $\theta_k$  for  $k = 1$  to  $K$ , where  $K < M$ . The data vector obtained by the AVS array at time  $t$  may be depicted as

$$\mathbf{x}(t) = \mathbf{A}(\boldsymbol{\theta})\mathbf{s}(t) + \mathbf{w}(t), \quad (1)$$

The output vector  $\mathbf{x}(t)$  of the AVS array has dimensions  $3M \times 1$ , with  $\mathbf{s}(t)$  representing the signal vector, and  $\mathbf{w}(t)$  representing the noise vector. Here,  $\mathbf{A}(\boldsymbol{\theta}) = [\mathbf{a}(\theta_1), \mathbf{a}(\theta_2), \dots, \mathbf{a}(\theta_K)]$  is the manifold matrix of the AVS array, where  $\mathbf{a}(\theta_k)$  can be expressed as

$$\mathbf{a}(\theta_k) = [a_{1p}(\theta_k) \otimes \mathbf{h}(\theta_k), \dots, a_{Mp}(\theta_k) \otimes \mathbf{h}(\theta_k)]^T, \quad (2)$$

with  $\mathbf{h}(\theta_k) = [1 \cos \theta_k \sin \theta_k]^T$ ,  $a_{mp}(\theta_k) = e^{-j2\pi(\frac{(m-1)d}{\lambda}) \cos \theta_k}$  the coefficient representing the response of acoustic pressure, where  $\lambda$  signifies the signal's wavelength.

### B. The AVS Array Model under TVAD

In real-world applications, the APV sensor is commonly attached to the bracket with a flexible connection, in contrast to the APS, which is usually rigidly connected to the bracket. Consequently, due to the influence of various complex marine environmental factors, including buoyancy effects and ocean currents, etc., the axial orientation of the APV sensor may undergo random changes, which may result in the axial deviation of each APV sensor being time-varying.

Suppose  $T$  represents the total time of collecting data,  $L$  indicates the number of snapshots collected by AVS array within the total time of collecting data, and  $Z$  denotes the number of equal-length sub-time period (STP) within the total time of collecting data. In order to model the time-varying axial angle deviation of AVS array in practical engineering application, it is a reasonable assumption that the axial angle deviation of each APV sensor is different within each STP. The vector  $\boldsymbol{\beta}_z = [\beta_{1z}, \beta_{2z}, \dots, \beta_{Mz}]$  represents the TVAD in the  $z$ th STP, where  $\beta_{mz}$  denotes the angular divergence along the longitudinal direction of the  $m$ th AVS. The AVS array model under TVAD in the  $z$ th STP is depicted in Fig. 1(b). Given the conditions, the multiple array matrix of the  $m$ th AVS in the  $z$ th STP for the  $k$ th incoming signal source can be represented as

$$\begin{aligned} \mathbf{h}(\theta_k, \beta_{mz}) &= \begin{bmatrix} 1 \\ \cos(\theta_k - \beta_{mz}) \\ \sin(\theta_k - \beta_{mz}) \end{bmatrix} \\ &= \begin{bmatrix} 1 \\ \cos \theta_k \cos \beta_{mz} + \sin \theta_k \sin \beta_{mz} \\ \sin \theta_k \cos \beta_{mz} - \cos \theta_k \sin \beta_{mz} \end{bmatrix} \quad (3) \\ &= \mathbf{c}_{mz} \mathbf{h}(\theta_k), \end{aligned}$$

with

$$\mathbf{c}_{mz} = \begin{bmatrix} 1 & 0 & 0 \\ 0 & \cos \beta_{mz} & \sin \beta_{mz} \\ 0 & -\sin \beta_{mz} & \cos \beta_{mz} \end{bmatrix}. \quad (4)$$

It is easy to find that

$$\mathbf{c}_{mz} \mathbf{c}_{mz}^H = \mathbf{c}_{mz}^H \mathbf{c}_{mz} = \mathbf{E}_3. \quad (5)$$

Then, in the  $z$ th STP, the planar array matrix of AVS is expressed below

$$\mathbf{A}(\boldsymbol{\theta}, \boldsymbol{\beta}_z) = [\mathbf{a}(\theta_1, \boldsymbol{\beta}_z), \mathbf{a}(\theta_2, \boldsymbol{\beta}_z), \dots, \mathbf{a}(\theta_K, \boldsymbol{\beta}_z)], \quad (6)$$

with

$$\begin{aligned} \mathbf{a}(\theta_k, \boldsymbol{\beta}_z) &= [\mathbf{a}(\theta_k, \boldsymbol{\beta}_z), \dots, \mathbf{a}(\theta_k, \boldsymbol{\beta}_z)]^T \\ &= [a_{1p}(\theta_k) \otimes \mathbf{h}(\theta_k, \beta_{1z}), \dots, a_{Mp}(\theta_k) \otimes \mathbf{h}(\theta_k, \beta_{Mz})]^T \\ &= [a_{1p}(\theta_k) \otimes (\mathbf{c}_{1z} \mathbf{h}(\theta_k)), \dots, a_{Mp}(\theta_k) \otimes (\mathbf{c}_{Mz} \mathbf{h}(\theta_k))]^T \\ &= [\mathbf{c}_{1z} (a_{1p}(\theta_k) \otimes \mathbf{h}(\theta_k)), \dots, \mathbf{c}_{Mz} (a_{Mp}(\theta_k) \otimes \mathbf{h}(\theta_k))]^T \\ &= \mathbf{C}_z \mathbf{a}(\theta_k), \end{aligned} \quad (7)$$

$$\mathbf{C}_z = blkdiag\{\mathbf{c}_{1z}, \mathbf{c}_{2z}, \dots, \mathbf{c}_{Mz}\}, \quad (8)$$

where  $\mathbf{C}_z$  denotes the TVAD matrix in the  $z$ th STP. Based on (5) and (8), we have

$$\mathbf{C}_z \mathbf{C}_z^H = \mathbf{C}_z^H \mathbf{C}_z = \mathbf{E}_{3M}. \quad (9)$$

Subsequently, the measurement data obtained by the AVS array with the TVAD in the  $z$ th STP at time  $t$  can be further converted into

$$\mathbf{x}_z(t) = \mathbf{A}(\boldsymbol{\theta}, \boldsymbol{\beta}_z) \mathbf{s}_z(t) + \mathbf{w}_z(t) = \mathbf{C}_z \mathbf{A}(\boldsymbol{\theta}) \mathbf{s}_z(t) + \mathbf{w}_z(t). \quad (10)$$

Suppose  $L_z$  and  $L_s$  represent the number of snapshot within each STP and the sampling time interval respectively. Based on the above statement, we can get  $L_z = L/Z$ . Next, we can express the  $z$ th STP's outcome vector of the AVS grid as

$$\mathbf{X}_z = \mathbf{C}_z \mathbf{A}(\boldsymbol{\theta}) \mathbf{S}_z + \mathbf{W}_z, \quad (11)$$

where  $\mathbf{X}_z = [\mathbf{x}_z(L_s), \mathbf{x}_z(2L_s), \dots, \mathbf{x}_z(L_z L_s)]$ ,  $\mathbf{S}_z = [\mathbf{s}_z(L_s), \mathbf{s}_z(2L_s), \dots, \mathbf{s}_z(L_z L_s)]$ , and  $\mathbf{W}_z = [\mathbf{w}_z(L_s), \mathbf{w}_z(2L_s), \dots, \mathbf{w}_z(L_z L_s)]$ .

In the spatial angle range of  $(-180^\circ \sim 180^\circ]$ , uniformly discretized into  $N$  discrete grids, each grid signifies a potential signal location. Then, the set of all possible incoming wave directions of signal sources within the spatial angle range is shown as  $\tilde{\boldsymbol{\theta}} = \{\tilde{\theta}_1, \tilde{\theta}_2, \dots, \tilde{\theta}_N\}$ , following the condition of  $N \gg K$  and  $\theta_k \in \tilde{\boldsymbol{\theta}}$ . Then, (11) can be reformulated as

$$\mathbf{X}_z = \mathbf{C}_z \mathbf{A}(\tilde{\boldsymbol{\theta}}) \tilde{\mathbf{S}}_z + \mathbf{W}_z, \quad (12)$$

where  $\tilde{\mathbf{S}}_z = [\tilde{\mathbf{s}}_{z1}, \tilde{\mathbf{s}}_{z2}, \dots, \tilde{\mathbf{s}}_{zN}]^T$  and  $\mathbf{W}_z = [\mathbf{w}_{z1}, \mathbf{w}_{z2}, \dots, \mathbf{w}_{z3M}]^T$ . Assuming uncorrelated signal and noise components, the covariance matrix of (12) is represented as

$$\mathbf{R}_z = E[\mathbf{X}_z \mathbf{X}_z^H] = \mathbf{C}_z \mathbf{A}(\tilde{\boldsymbol{\theta}}) \mathbf{P}_z \mathbf{A}^H(\tilde{\boldsymbol{\theta}}) \mathbf{C}_z^H + \mathbf{Q}_z, \quad (13)$$

where  $\tilde{\mathbf{P}}_z$  and  $\mathbf{Q}_z$  are the signal and noise covariance matrices in the  $z$ th STP, respectively. Specifically,

$$\tilde{\mathbf{P}}_z = E\{\tilde{\mathbf{S}}_z \tilde{\mathbf{S}}_z^H\} = diag\{\tilde{p}_{z1}^2, \tilde{p}_{z2}^2, \dots, \tilde{p}_{zN}^2\}, \quad (14)$$

and

$$\begin{aligned} \mathbf{Q}_z &= E\{\mathbf{W}_z \mathbf{W}_z^H\} \\ &= diag\{\sigma_{z1p}^2, \sigma_{z1x}^2, \sigma_{z1y}^2, \dots, \sigma_{zMp}^2, \sigma_{zMx}^2, \sigma_{zMy}^2\}, \end{aligned} \quad (15)$$

where  $\tilde{p}_{zn}^2 = \frac{1}{L_z} \tilde{\mathbf{s}}_{zn} \tilde{\mathbf{s}}_{zn}^H$ , and  $\sigma_{zmp}^2, \sigma_{zmx}^2, \sigma_{zmy}^2$  represent the noise power received for the APS and the two APVs of the  $m$ th AVS in the  $z$ th STP, respectively.

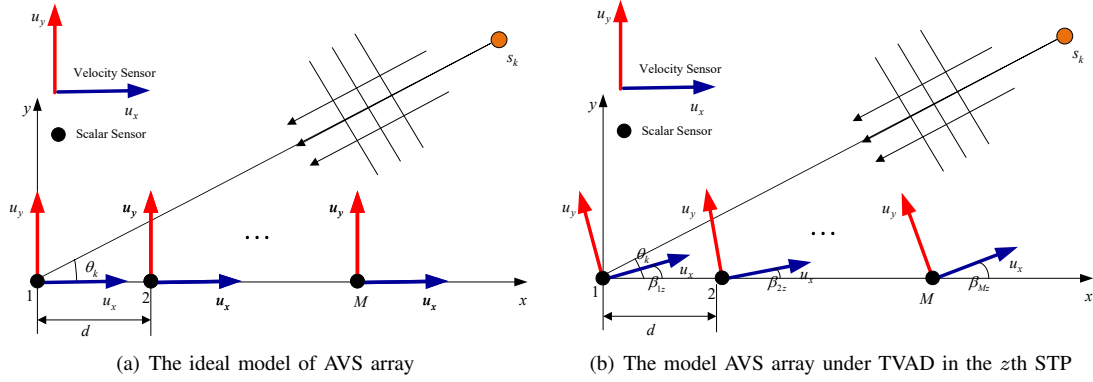


Fig. 1. The two measurement models of AVS array.

In real-world engineering endeavors, every link of an AVS grid is likely to receive a different amount of noise power because of the directivity of AVS and the non-ideality of AVS channel reaction. As stated in [22], [30], [32], [33], it is named as uniform noise if the noise variance of each channel for every AVS in the array is the same, that is,  $\{\sigma_{zmp}^2 = \sigma_{zmx}^2 = \sigma_{zmy}^2\}_{z=0}^Z = \sigma^2$ , it is named as ambient noise if  $\{\sigma_{zmp}^2\}_{z=0}^Z = \sigma_p^2$ ,  $\{\sigma_{zmv}^2\}_{z=0}^Z = \sigma_v^2$ , and  $\sigma_{mp}^2 = \sigma^2 \neq \sigma_{mv}^2$  are satisfied for every AVS in the array, and it is named as non-uniform noise if the noise variance of each channel for a single AVS is different and the noise variance of components between different AVSs in the array also varies, that is,  $\sigma_{z1p}^2 \neq \sigma_{z1x}^2 \neq \sigma_{z1y}^2 \neq \dots \neq \sigma_{zMp}^2 \neq \sigma_{zMx}^2 \neq \sigma_{zMy}^2 \neq \sigma^2$ .

Over the entire observation period, the output vector of AVS array is defined as

$$\mathbf{X} = [\mathbf{X}_0, \mathbf{X}_1, \dots, \mathbf{X}_z, \dots, \mathbf{X}_{Z-1}]. \quad (16)$$

It can be seen from (11) and (16) that there are different axial deviations in each STP. Due to the existence of TVAD in the data collected throughout the entire observation period, these existing methods suffer from severe performance degradation if the collected data throughout the entire observation period is used directly to predict the DOA of target. Furthermore, in (15), the disparate levels of noise power in individual channels within the AVS array may lead to a significant degradation in the performance of DOA estimation. Consequently, an innovative DOA computation paradigm is introduced in the following portion in order to precisely estimate the DOAs of underwater targets.

### III. THE PROPOSED TECHNIQUE

This part of the study reconstructs the cost function for the TVAD matrix using the technique of weighted least squares. Due to the involvement of user parameters, the cost of reconstruction is a nonlinear function of the TVAD matrix. The TVAD matrix's nonlinear form was then converted into a linear relationship using the majorization-minimization algorithm [34], and the analytical expression of the matrix was quantified. Secondly, leveraging the estimated TVAD matrix, we modified the data within each STP the effect of axial deviation on the DOA prediction accuracy of the AVS array.

Following this, based on the modified STP data, we introduce a novel manifold matrix for the AVS array, treating the noise output vectors from its  $3M$  channels as potential sparse signals. Finally, based on the newly formed AVS array data model, we reconstruct the cost function for joint estimation of potential sparse signals.

Assuming that there is no noise term in (12). Then, the received data of AVS array in the  $z$ th STP can be expressed by

$$\mathbf{X}_{sz} = \mathbf{C}_z \mathbf{A}(\tilde{\theta}) \tilde{\mathbf{S}}_z. \quad (17)$$

By multiplying both sides of (17) by  $\mathbf{C}_z^H$  yields

$$\mathbf{C}_z^H \mathbf{X}_{sz} = \mathbf{A}(\tilde{\theta}) \tilde{\mathbf{S}}_z. \quad (18)$$

Considering that it is easier to obtain the axial deviation of AVS array at the beginning or end of data acquisition when AVS array collects data in underwater. Therefore, we will take the data of the initial STP (located at the first STP) as a reference. In the  $z$ th STP, the AVS array's collected data, free from noise and axial deviation, can be represented as

$$\mathbf{C}_z^H \mathbf{X}_{sz} = \mathbf{X}_{s0}. \quad (19)$$

The output data of the AVS array in the absence of noise in the reference STP is denoted by  $\mathbf{X}_{s0}$ . In the case of the existence of noise, the singular value decomposition (SVD) of the data obtained from the  $z$ th STP can be articulated as

$$\mathbf{X}_z = \mathbf{U}_z \mathbf{\Sigma}_z \mathbf{V}_z^H. \quad (20)$$

Assuming that the number of signal sources has been detected by using the method proposed in [35]. Then, the first  $K$  elements on the diagonal of the right singular vectors  $\mathbf{V}_z$  are utilized to reconstruct  $\mathbf{X}_{sz}$  in practical applications. Let  $\mathbf{D}_z = \text{diag}\{\mathbf{1}_K, \mathbf{0}_{L_z-K}\}$ , where  $\mathbf{1}_K$  represents a vector consisting of  $K$  elements of 1 and  $\mathbf{0}_{L_z-K}$  represents a vector consisting of  $L_z - K$  elements of 0. Similar to the statement in [36], we have

$$\mathbf{X}_{sz} = \mathbf{X}_z \mathbf{V}_z \mathbf{D}_z. \quad (21)$$

It is noted that the product of  $\mathbf{X}_{w0}$  and  $\mathbf{X}_0 - \mathbf{C}_z^H \mathbf{X}_{sz}$  may be the matrix identity if we can obtain the true value of the TVAD matrix  $\mathbf{C}_z$ .

Thus, in the fist step, by fitting the signal and noise subspaces, the cost matrix for the TVAD matrix was reconstructed

to estimate the TVAD matrix while keeping the sparse signal fixed,

$$\mathbf{C}_z^{(j+1)} = \arg \min f(\mathbf{C}_z), \quad (22)$$

with

$$f(\mathbf{C}_z) = \left\| \mathbf{X}_{w0}^\dagger (\mathbf{X}_{s0} - \mathbf{C}_z^H \mathbf{X}_{sz}) \right\|_F^2 + \lambda_c \|\mathbf{C}_z\|_F^q, \quad (23)$$

where the first term,  $\left\| \mathbf{X}_{w0}^\dagger (\mathbf{X}_{s0} - \mathbf{C}_z^H \mathbf{X}_{sz}) \right\|_F^2$ , is a fitting term that enforces consistency between the signal subspaces across different STPs, ensuring that the estimated TVAD matrix  $\mathbf{C}_z$  accurately compensates for axial deviations, the second term,  $\|\mathbf{C}_z\|_F^q$ , is a regularization term with two key components: (1) the Frobenius norm ( $\|\mathbf{C}_z\|_F$ ) measures the “magnitude” of the TVAD matrix  $\mathbf{C}_z$ , which is block-diagonal and composed of rotation matrices  $\mathbf{c}_{mz}$ ; (2) the exponent  $q$  controls the sparsity of axial deviations and strikes a balance between sparsity and computational tractability. When  $0 < q < 1$ , this term promotes sparsity in the deviations, implying that only a subset of AVS elements exhibit significant axial deviations. For  $q = 1$ , it reduces to the Lasso penalty, encouraging sparsity but with less selectivity. Noting that the second term,  $\|\mathbf{C}_z\|_F^q$ , penalizes large deviations in  $\mathbf{C}_z$ , ensuring that the estimated axial deviations are physically plausible, and  $\lambda_c$  balances the trade-off between the first term and the second term.

Once  $\hat{\mathbf{C}}_z$  is obtained, the received data from different STP can be modified as

$$\mathbf{X}_z^{(j+1)} = \hat{\mathbf{C}}_z^{H(j+1)} \mathbf{X}_z^{(j)}. \quad (24)$$

The noise power inequality given in (15) is expected to significantly degrade the DOA prediction efficiency of the AVS array. To tackle this challenge, we establish a fresh planar matrix for the AVS array as  $\mathbf{B}_z$  in  $z$ th STP, and  $\mathbf{B}_z$  is denoted as

$$\mathbf{B}_z = [\mathbf{C}_z \mathbf{A}_1, \mathbf{C}_z \mathbf{A}_2, \dots, \mathbf{C}_z \mathbf{A}_r, \dots, \mathbf{C}_z \mathbf{A}_N, \mathbf{E}_{3M}], \quad (25)$$

with  $\mathbf{A}_r$  being the  $r$ th column of  $\mathbf{A}(\tilde{\theta})$ . Therefor, (12) is updated as

$$\mathbf{X}_z = \mathbf{B}_z \bar{\mathbf{S}}_z, \quad (26)$$

where

$$\bar{\mathbf{S}}_z = \begin{bmatrix} \tilde{\mathbf{S}}_z \\ \mathbf{W}_z \end{bmatrix} = [\bar{s}_{z1}, \bar{s}_{z1}, \dots, \bar{s}_{zr}, \dots, \bar{s}_{z(N+3M)}]^T. \quad (27)$$

From (26), it is evident that  $\mathbf{B}_z$  consists of the manifold matrix representing the actual AVS array manifold matrix and an identity matrix. The manifold matrix of the actual AVS array is utilized for estimating the sparse signal, while the identity matrix is employed for estimating the noise vector. Then, (13) can be further transformed into

$$\mathbf{R}_z = E[\mathbf{X}_z \mathbf{X}_z^H] = \mathbf{B}_z \mathbf{\Xi}_z \mathbf{B}_z^H, \quad (28)$$

with

$$\begin{aligned} \mathbf{\Xi}_z &= \begin{bmatrix} \tilde{\mathbf{p}}_z & \mathbf{0}_{N \times 3M} \\ \mathbf{0}_{N \times 3M}^T & \mathbf{Q}_z \end{bmatrix} \\ &= \begin{bmatrix} \bar{p}_{z1} & 0 & \dots & \dots & 0 \\ 0 & \ddots & \vdots & \vdots & \vdots \\ \vdots & \vdots & \bar{p}_{zr} & \vdots & \vdots \\ 0 & \dots & \dots & \ddots & 0 \\ 0 & \dots & \dots & 0 & \bar{p}_{z(N+3M)} \end{bmatrix}. \end{aligned} \quad (29)$$

Noting that the first  $N$  elements along the diagonal of  $\mathbf{\Xi}_z$  correspond to sparse signal power, whereas elements  $N+1$  to  $N+3M$  related to noise power. Let  $\mathbf{R}_{zr}$  and  $\mathbf{\Gamma}_{zr}$  be the signal covariance matrix and the interference and noise covariance matrix from the  $r$ th grid in  $z$ th STP, respectively. Then, we have

$$\mathbf{R}_{zr} = \bar{p}_{zr} \mathbf{B}_{zr} \mathbf{B}_{zr}^H, \quad (30)$$

and

$$\mathbf{\Gamma}_{zr} = \mathbf{R}_z - \mathbf{R}_{zr} = \mathbf{B}_z \mathbf{\Xi}_z \mathbf{B}_z^H - \mathbf{R}_{zr}. \quad (31)$$

Then, in the second step, utilizing the techniques of regularized weighted least squares and fitting the interference and noise covariance matrix, we formulate a cost function aimed at concurrently estimating the power of sparse signals and noise as

$$\bar{\mathbf{s}}_{zr}^{(j+1)} = \arg \min f(\bar{\mathbf{s}}_{zr}), \quad (32)$$

with

$$f(\bar{\mathbf{s}}_{zr}) = \left\| \mathbf{\Gamma}_{zr}^{-0.5(j+1)} (\mathbf{X}_{sz}^{(j)} - \mathbf{B}_{zr} \bar{\mathbf{s}}_{zr}^{(j)}) \right\|_F^2 + \lambda_s \|\bar{\mathbf{s}}_{zr}\|_F^q, \quad (33)$$

where the former term and the latter term in (33) indicate the weighted least squares fitting term and a penalty notion that enforces the signal’s sparsity,  $\lambda_s > 0$  denotes the fitting loss and sparse data regularization, and  $q$  constraining the sparsity of signal. In the following subsection, we will introduce how to solve TVAD matrix and an the power of sparse signal and noise from (23) and (33).

#### A. Estimating the TVAD Matrix

It is noted that the cost function  $f(\mathbf{C}_z)$  for the TVAD matrix  $\mathbf{C}_z$  in (23) is a nonlinear function due to the term  $\|\mathbf{C}_z\|_F^q$  with a user parameter  $q$ . Thus, directly solving for the TVAD matrix  $\mathbf{C}_z$  from the cost function  $f(\mathbf{C}_z)$  in (23) is challenging. To handle the nonlinearity, we employ the Majorization-Minimization (MM) algorithm [34], which iteratively majorizes the nonlinear term  $\|\mathbf{C}_z\|_F^q$  with a linear surrogate function.

Let  $\|\mathbf{C}_z\|_F^2$  is an separate parameter in  $(\|\mathbf{C}_z\|_F^2)^{\frac{q}{2}}$  and  $\|\mathbf{C}_z^{(j)}\|_F^2$  is the estimated outcome of the  $j$ th cycle according to  $\|\mathbf{C}_z\|_F^2$ . Based on the MM algorithm [34] and the statement in [37], the nonlinear term is approximated using the first-order Taylor expansion around the current estimate  $\mathbf{C}_z^{(j)}$ ,

$$\begin{aligned} \left( \|\mathbf{C}_z\|_F^2 \right)^{\frac{q}{2}} &\leq \left( \|\mathbf{C}_z^{(j)}\|_F^2 \right)^{\frac{q}{2}} + \frac{q}{2} \left( \|\mathbf{C}_z^{(j)}\|_F^2 \right)^{\left( \frac{q}{2}-1 \right)} \\ &\quad \times \left( \|\mathbf{C}_z\|_F^2 - \|\mathbf{C}_z^{(j)}\|_F^2 \right). \end{aligned} \quad (34)$$

This approximation converts the original nonlinear optimisation problem into a series of linear subproblems to solve. Then, multiplying  $\lambda_c$  and then adding  $\left\| \mathbf{X}_{w0}^\dagger (\mathbf{X}_0 - \mathbf{C}_z^H \mathbf{X}_{sz}) \right\|_F^2$  on both sides of (34), we get

$$f(\mathbf{C}_z) \leq h(\mathbf{C}_z), \quad (35)$$

with

$$\begin{aligned} h(\mathbf{C}_z) &= \left\| \mathbf{X}_{w0}^\dagger (\mathbf{X}_0 - \mathbf{C}_z^H \mathbf{X}_{sz}) \right\|_F^2 + \lambda_c \left( \left\| \mathbf{C}_z^{(j)} \right\|_F^2 \right)^{\frac{q}{2}} \\ &\quad + \frac{q\lambda_c}{2} \left( \left\| \mathbf{C}_z^{(j)} \right\|_F^2 \right)^{\left(\frac{q}{2}-1\right)} \left( \left\| \mathbf{C}_z \right\|_F^2 - \left\| \mathbf{C}_z^{(j)} \right\|_F^2 \right). \end{aligned} \quad (36)$$

It is worth noting that  $\mathbf{C}_z^{(j)}$  in (36) is a definite value because it is collected in the  $j$ th cycle. Then, minima of (22) is further comparable to the following equation's minimisation with regard to  $\mathbf{C}_z$

$$\mathbf{C}_z = \arg \min F(\mathbf{C}_z), \quad (37)$$

with

$$\begin{aligned} F(\mathbf{C}_z) &= \left\| \mathbf{X}_{w0}^\dagger (\mathbf{X}_0 - \mathbf{C}_z^H \mathbf{X}_{sz}) \right\|_F^2 \\ &\quad + \frac{q\lambda_c}{2} \left( \left\| \mathbf{C}_z^{(j)} \right\|_F^2 \right)^{\left(\frac{q}{2}-1\right)} \left\| \mathbf{C}_z \right\|_F^2. \end{aligned} \quad (38)$$

Based on the properties of the Frobenius norm [38], (38) is modified as

$$\begin{aligned} F(\mathbf{C}_z) &= \text{Trace} \left\{ \left( \mathbf{X}_{w0}^\dagger (\mathbf{X}_0 - \mathbf{C}_z^H \mathbf{X}_{sz}) \right)^H \right. \\ &\quad \times \left. \left( \mathbf{X}_{w0}^\dagger (\mathbf{X}_0 - \mathbf{C}_z^H \mathbf{X}_{sz}) \right) \right\} \\ &\quad + \frac{q\lambda_c}{2} \left( \left\| \mathbf{C}_z^{(j)} \right\|_F^2 \right)^{\left(\frac{q}{2}-1\right)} \text{Trace} \left\{ \mathbf{C}_z^H \mathbf{C}_z \right\} \\ &= \text{Trace} \left\{ \mathbf{X}_0^H (\mathbf{X}_{w0}^\dagger)^H \mathbf{X}_{w0}^\dagger \mathbf{X}_0 \right\} \\ &\quad - 2 \text{Trace} \left\{ \mathbf{X}_0^H (\mathbf{X}_{w0}^\dagger)^H \mathbf{X}_{w0}^\dagger \mathbf{C}_z^H \mathbf{X}_{sz} \right\} \\ &\quad + \text{Trace} \left\{ \mathbf{X}_{sz}^H \mathbf{C}_z (\mathbf{X}_{w0}^\dagger)^H \mathbf{X}_{w0}^\dagger \mathbf{C}_z^H \mathbf{X}_{sz} \right\} \\ &\quad + \frac{q\lambda_c}{2} \left( \left\| \mathbf{C}_z^{(j)} \right\|_F^2 \right)^{\left(\frac{q}{2}-1\right)} \text{Trace} \left\{ \mathbf{C}_z^H \mathbf{C}_z \right\}. \end{aligned} \quad (39)$$

Now, we will compute the first-order differential form of the second, third, and final terms in (39) in accordance with  $\mathbf{C}_z$ . Using the properties of matrix derivatives, the following expression is obtained

$$\begin{aligned} &\mathcal{D} \left( \text{Trace} \left\{ \mathbf{X}_0^H (\mathbf{X}_{w0}^\dagger)^H \mathbf{X}_{w0}^\dagger \mathbf{C}_z^H \mathbf{X}_{sz} \right\} \right) \\ &= \text{Trace} \left\{ \mathbf{X}_{sz} \mathbf{X}_0^H (\mathbf{X}_{w0}^\dagger)^H \mathbf{X}_{w0}^\dagger \mathcal{D} (\mathbf{C}_z^H) \right\} \\ &= \text{Trace} \left\{ \left( \mathbf{X}_{sz} \mathbf{X}_0^H (\mathbf{X}_{w0}^\dagger)^H \mathbf{X}_{w0}^\dagger \right)^H \mathcal{D} (\mathbf{C}_z) \right\}, \end{aligned} \quad (40)$$

$$\begin{aligned} &\mathcal{D} \left( \text{Trace} \left\{ \mathbf{X}_{sz}^H \mathbf{C}_z (\mathbf{X}_{w0}^\dagger)^H \mathbf{X}_{w0}^\dagger \mathbf{C}_z^H \mathbf{X}_{sz} \right\} \right) \\ &= \text{Trace} \left\{ \mathbf{X}_{sz}^H \mathcal{D} (\mathbf{C}_z) (\mathbf{X}_{w0}^\dagger)^H \mathbf{X}_{w0}^\dagger \mathbf{C}_z^H \mathbf{X}_{sz} \right\} \\ &\quad + \text{Trace} \left\{ \mathbf{X}_{sz}^H \mathbf{C}_z (\mathbf{X}_{w0}^\dagger)^H \mathbf{X}_{w0}^\dagger \mathcal{D} (\mathbf{C}_z^H) \mathbf{X}_{sz} \right\} \\ &= 2 \text{Trace} \left\{ (\mathbf{X}_{w0}^\dagger)^H \mathbf{X}_{w0}^\dagger \mathbf{X}_{sz} \mathbf{X}_{sz}^H \mathbf{C}_z^H \mathcal{D} (\mathbf{C}_z) \right\}, \end{aligned} \quad (41)$$

and

$$\begin{aligned} &\mathcal{D} \left( \frac{q\lambda_c}{2} \left( \left\| \mathbf{C}_z^{(j)} \right\|_F^2 \right)^{\left(\frac{q}{2}-1\right)} \mathbf{C}_z^H \mathbf{C}_z \right) \\ &= \frac{q\lambda_c}{2} \left( \left\| \mathbf{C}_z^{(j)} \right\|_F^2 \right)^{\left(\frac{q}{2}-1\right)} (\mathcal{D} (\mathbf{C}_z^H) \mathbf{C}_z + \mathbf{C}_z^H \mathcal{D} (\mathbf{C}_z)) \\ &= q\lambda_c \left( \left\| \mathbf{C}_z^{(j)} \right\|_F^2 \right)^{\left(\frac{q}{2}-1\right)} \mathbf{C}_z^H \mathcal{D} (\mathbf{C}_z). \end{aligned} \quad (42)$$

Subsequently, we obtain the first derivation of  $F(\mathbf{C}_z)$  regarding to  $\mathbf{C}_z$ ,

$$\begin{aligned} \frac{\partial F(\mathbf{C}_z)}{\partial \mathbf{C}_z} &= -2 \mathbf{X}_{sz} \mathbf{X}_0^H (\mathbf{X}_{w0}^\dagger)^H \mathbf{X}_{w0}^\dagger \\ &\quad + 2 \mathbf{X}_{sz} \mathbf{X}_{sz}^H (\mathbf{X}_{w0}^\dagger)^H \mathbf{X}_{w0}^\dagger \mathbf{C}_z \\ &\quad + q\lambda_c \left( \left\| \mathbf{C}_z^{(j)} \right\|_F^2 \right)^{\left(\frac{q}{2}-1\right)} \mathbf{C}_z, \end{aligned} \quad (43)$$

By setting  $\frac{\partial F(\mathbf{C}_z)}{\partial \mathbf{C}_z} = \mathbf{0}$ , we have

$$\begin{aligned} &-2 \mathbf{X}_{sz} \mathbf{X}_0^H (\mathbf{X}_{w0}^\dagger)^H \mathbf{X}_{w0}^\dagger + 2 \mathbf{X}_{sz} \mathbf{X}_{sz}^H (\mathbf{X}_{w0}^\dagger)^H \mathbf{X}_{w0}^\dagger \mathbf{C}_z \\ &+ q\lambda_c \left( \left\| \mathbf{C}_z^{(j)} \right\|_F^2 \right)^{\left(\frac{q}{2}-1\right)} \mathbf{C}_z = \mathbf{0}. \end{aligned} \quad (44)$$

By isolating the terms involving  $\mathbf{C}_z$ , we get

$$\begin{aligned} &2 \mathbf{X}_{sz} \mathbf{X}_{sz}^H (\mathbf{X}_{w0}^\dagger)^H \mathbf{X}_{w0}^\dagger \mathbf{C}_z + q\lambda_c \left( \left\| \mathbf{C}_z^{(j)} \right\|_F^2 \right)^{\left(\frac{q}{2}-1\right)} \mathbf{C}_z \\ &= 2 \mathbf{X}_{sz} \mathbf{X}_0^H (\mathbf{X}_{w0}^\dagger)^H \mathbf{X}_{w0}^\dagger. \end{aligned} \quad (45)$$

Then, the left-hand side can be factored as

$$\begin{aligned} &\left( 2 \mathbf{X}_{sz} \mathbf{X}_{sz}^H (\mathbf{X}_{w0}^\dagger)^H \mathbf{X}_{w0}^\dagger + q\lambda_c \left( \left\| \mathbf{C}_z^{(j)} \right\|_F^2 \right)^{\left(\frac{q}{2}-1\right)} \mathbf{E} \right) \mathbf{C}_z \\ &= 2 \mathbf{X}_{sz} \mathbf{X}_0^H (\mathbf{X}_{w0}^\dagger)^H \mathbf{X}_{w0}^\dagger. \end{aligned} \quad (46)$$

Suppose the estimate for  $\mathbf{C}_z$  is marked  $\hat{\mathbf{C}}_z^{(j+1)}$  on the  $(j+1)$ th cycle. After that we got

$$\mathbf{C}_z^{(j+1)} = \frac{\mathbf{v}^{(j)}}{\tau^{(j)} + q\lambda_c \left( \left\| \mathbf{C}_z^{(j)} \right\|_F^2 \right)^{\left(\frac{q}{2}-1\right)} \mathbf{E}}, \quad (47)$$

with

$$\mathbf{v}^{(j)} = 2 \mathbf{X}_{sz}^{(j)} \mathbf{X}_0^H (\mathbf{X}_{w0}^\dagger)^H \mathbf{X}_{w0}^\dagger, \quad (48)$$

and

$$\tau^{(j)} = 2 \mathbf{X}_{sz}^{(j)} \mathbf{X}_{sz}^H (\mathbf{X}_{w0}^\dagger)^H \mathbf{X}_{w0}^\dagger. \quad (49)$$

After  $\hat{\mathbf{C}}_z^{(j+1)}$  is obtained, the received data of AVS array for each STP is modified as

$$\mathbf{X}_z^{(j+1)} = \hat{\mathbf{C}}_z^{H(j+1)} \mathbf{X}_z^{(j)}. \quad (50)$$

It is evident that combining the dataset processed by matrix focusing technology with existing DOA estimation methods can further enhance the accuracy of DOA estimation for AVS

array under TVAD. However, the DOA estimation performance of AVS array may still suffer from significant degradation due to the impact of non-uniform noise. To overcome this issue, enhanced DOA estimation techniques need to be presented to achieve better estimation performance

### B. Estimating the Power of Signal and Noise

Based on (23) and (33), it can be seen that the cost functions have a similar structural form with respect to the independent variables. Thus, the cost function for  $\tilde{\mathbf{S}}_z$  in (33) is inherently nonlinear due to the user-defined parameter  $q$ , making the direct solution of  $\bar{\mathbf{s}}_{zr}$  from (33) computationally challenging. By using the algorithm [34] and following the derivations in (34)–(38), the minimization of (32) over  $\{\bar{\mathbf{s}}_{zr}\}_{r=1}^{N+3M}$  simplifies to

$$\bar{\mathbf{s}}_{zr}^{(j+1)} = \arg \min F(\bar{\mathbf{s}}_{zr}), \quad (51)$$

with

$$\begin{aligned} F(\bar{\mathbf{s}}_{zr}) &= \left\| \mathbf{\Gamma}_{zr}^{-0.5(j)} \left( \mathbf{X}_{sz}^{(j)} - \mathbf{B}_{zr} \bar{\mathbf{s}}_{zr} \right) \right\|_F^2 \\ &\quad + \frac{q\lambda_s}{2} \left( \left\| \bar{\mathbf{s}}_{zr}^{(j)} \right\|_F^2 \right)^{\frac{q}{2}} \left\| \bar{\mathbf{s}}_{zr} \right\|^2. \end{aligned} \quad (52)$$

From (52), we can find that the auxiliary function  $F(\bar{\mathbf{s}}_{zr})$  is a linear function about the variable  $\bar{\mathbf{s}}_{zr}$ . Therefore,  $\bar{\mathbf{s}}_{zr}$  can be directly solved from (52) by solving the first derivative of the auxiliary function  $F(\bar{\mathbf{s}}_{zr})$  with respect to  $\bar{\mathbf{s}}_{zr}$  and setting the first derivative to zero.

Then, we can obtain the first-order and second-order derivatives of  $F(\bar{\mathbf{s}}_{zr})$ , respectively,

$$\begin{aligned} \frac{\partial F(\bar{\mathbf{s}}_{zr})}{\partial \bar{\mathbf{s}}_{zr}} &= 2 \left( \bar{\mathbf{s}}_{zr}^H \mathbf{B}_{zr}^H \mathbf{\Gamma}_{zr}^{-1(j)} \mathbf{B}_{zr} \right)^H \\ &\quad - 2 \left( \mathbf{X}_{sz}^{(j)} \mathbf{\Gamma}_{zr}^{-1(j)} \mathbf{B}_{zr} \right)^H + q\lambda_s \left( \left\| \bar{\mathbf{s}}_{zr}^{(j)} \right\|_F^2 \right)^{\frac{q}{2}} \bar{\mathbf{s}}_{zr}, \end{aligned} \quad (53)$$

and

$$\frac{\partial^2 F(\bar{\mathbf{s}}_{zr})}{\partial \bar{\mathbf{s}}_{zr}} = 2 \mathbf{B}_{zr}^H \mathbf{\Gamma}_{zr}^{-1(j)} \mathbf{B}_{zr} + p\lambda_s \left( \left\| \bar{\mathbf{s}}_{zr}^{(j)} \right\|_F^2 \right)^{\frac{q}{2}}. \quad (54)$$

Let  $\partial F(\bar{\mathbf{s}}_{zr})/\partial \bar{\mathbf{s}}_{zr} = 0$ , we can update the estimation of  $\tilde{\mathbf{S}}_z$  at the  $(j+1)$ th iteration as

$$\hat{\mathbf{s}}_{zr}^{(j+1)} = \frac{\mathbf{B}_{zr}^H \mathbf{\Gamma}_{zr}^{-1(j)} \mathbf{X}_{sz}^{(j)}}{\mathbf{B}_{zr}^H \mathbf{\Gamma}_{zr}^{-1(j)} \mathbf{B}_{zr} + \frac{q\lambda_s}{2} \left( \left\| \bar{\mathbf{s}}_{zr}^{(j)} \right\|_F^2 \right)^{\left(\frac{q}{2}-1\right)}}, \quad (55)$$

with

$$\begin{aligned} \mathbf{\Gamma}_{zr} &= \mathbf{R}_z - \mathbf{R}_{zr} = \mathbf{B}_z \mathbf{\Xi}_z \mathbf{B}_z^H - \mathbf{R}_{zr}, \\ r &= 1, 2, \dots, N, N+1, \dots, 3M. \end{aligned} \quad (56)$$

Substituting (56) into (55), we obtain

$$\hat{\mathbf{s}}_{zr}^{(j+1)} = \frac{\mathbf{B}_{zr}^H \mathbf{R}_z^{-1(j)} \mathbf{X}_{sz}^{(j+1)}}{\omega_z^{(j)} + \frac{q\lambda_s}{2} \left( \left\| \bar{\mathbf{s}}_{zr}^{(j)} \right\|_F^2 \right)^{\left(\frac{q}{2}-1\right)} \eta_z^{(j)}}, \quad (57)$$

where

$$\omega_z^{(j)} = \mathbf{B}_{zr}^H \mathbf{R}_z^{-1(j)} \mathbf{B}_{zr}, \quad (58)$$

$$\eta_z^{(j)} = 1 - \hat{p}_{zr}^{(j)} \mathbf{B}_{zr}^H \mathbf{R}_z^{-1(j)} \mathbf{B}_{zr}, \quad (59)$$

$$\mathbf{R}_z^{(j)} = \mathbf{A} \left( \tilde{\boldsymbol{\theta}} \right) \mathbf{P}_z^{(j)} \mathbf{A}^H \left( \tilde{\boldsymbol{\theta}} \right) + \hat{\mathbf{Q}}_z^{(j)}, \quad (60)$$

and

$$\hat{\mathbf{Q}}_z^{(j)} = \text{diag} \{ \hat{\sigma}_{z1}^{2(j)}, \hat{\sigma}_{z2}^{2(j)}, \dots, \hat{\sigma}_{z3M}^{2(j)} \}. \quad (61)$$

Therefore, the signal and noise vectors for the  $z$ th STP can be respectively updated as

$$\hat{\mathbf{S}}_z^{(j+1)} = [\hat{\mathbf{s}}_{z1}^{(j+1)}, \hat{\mathbf{s}}_{z2}^{(j+1)}, \dots, \hat{\mathbf{s}}_{zN}^{(j+1)}]^T, \quad (62)$$

and

$$\hat{\mathbf{W}}_z^{(j+1)} = [\hat{\mathbf{s}}_{z(N+1)}^{(j+1)}, \hat{\mathbf{s}}_{z(N+2)}^{(j+1)}, \dots, \hat{\mathbf{s}}_{z(N+3M)}^{(j+1)}]^T. \quad (63)$$

Then, the power of signal and the noise for the  $z$ th STP can be derived as

$$\begin{aligned} \hat{p}_{zr}^{(j+1)} &= E \{ \hat{\mathbf{s}}_{zr}^{(j+1)} \hat{\mathbf{s}}_{zr}^{H(j+1)} \}, \\ r &= 1, 2, \dots, N, \end{aligned} \quad (64)$$

and

$$\begin{aligned} \hat{\sigma}_{zl}^{2(j+1)} &= E \{ \mathbf{w}_{zl}^{(j+1)} \mathbf{w}_{zl}^{H(j+1)} \} = E \{ \hat{\mathbf{s}}_{zr}^{(j+1)} \hat{\mathbf{s}}_{zr}^{H(j+1)} \} \\ r &= N+1, N+2, \dots, N+3M, \\ l &= 1, 2, \dots, 3M. \end{aligned} \quad (65)$$

Based on (64) and (65), it is clear that  $\hat{p}_{zr}^{(0)}$  and  $\hat{\sigma}_{zl}^{(0)}$  are needed, where  $\hat{p}_n^{(0)}$  and  $\hat{\sigma}_{zl}^{2(0)}$  can be initialized by conventional beamforming method [39] and sparse asymptotic minimum variance method [38], respectively.

Throughout the entire observation period, the estimated signal vector and the signal power vector  $\hat{\mathbf{P}}^{(j+1)}$  can be respectively expressed as

$$\hat{\mathbf{S}}^{(j+1)} = [\hat{\mathbf{s}}_0^{(j+1)}, \hat{\mathbf{s}}_1^{(j+1)}, \dots, \hat{\mathbf{s}}_{Z-1}^{(j+1)}], \quad (66)$$

$$\hat{\mathbf{P}}^{(j+1)} = \text{diag} \{ E \{ \hat{\mathbf{S}}^{(j+1)} \hat{\mathbf{S}}^{H(j+1)} \} \}. \quad (67)$$

Ultimately, the DOAs of source can be determined by performing peak search on  $\hat{\mathbf{P}}^{(j+1)}$ . The proposed algorithm is summarized in Algorithm 1.

---

#### Algorithm 1 The proposed DOA estimation technology

---

**Input:**  $\mathbf{X}$ ,  $K$ ,  $\tilde{\boldsymbol{\theta}}$ ,  $Z$ .

**Initialization:**  $\hat{p}_{zr}^{(0)}$  and  $\hat{\sigma}_{zl}^{(0)}$  using conventional beamforming method [39] and sparse asymptotic minimum variance method [38];

**repeat:**

Calculate  $\mathbf{R}_z$  by (60);

Calculate  $\hat{\mathbf{C}}_z^{(j+1)}$  by (47);

Update  $\mathbf{X}_z^{(j+1)}$  by (50);

Calculate  $\hat{\mathbf{s}}_{zr}^{(j+1)}$  by (57);

Calculate  $\hat{p}_{zr}^{(j+1)}$  by (64);

Calculate  $\hat{\sigma}_{zl}^{2(j+1)}$  by (65);

Update  $\hat{\mathbf{P}}^{(j+1)}$  by (67);

Set  $j = j + 1$ ;

**Until:**  $\left\| \hat{\mathbf{P}}^{(j+1)} - \hat{\mathbf{P}}^{(j)} \right\|_F^2 / \left\| \hat{\mathbf{P}}^{(j)} \right\|_F^2 < \ell$  or  $j \geq T_{\max}$ .

**Output:**  $\hat{\boldsymbol{\theta}}_K$ .

---

#### IV. SIMULATION RESULTS

In this section, to verify the effectiveness and robustness of the proposed method, we compare it with these methods, including MUSIC [16], IAA [12], ASMUSIC [21], ANEMUSIC [22], iterative maximum-likelihood subspace estimation (IMLSE) [26] and CMFF [31]. The Cramer-Rao lower bound (CRLB) [40] is depicted as a reference standard for evaluating the performance of DOA estimation. Unless otherwise specified in the simulation, the AVS array with  $M = 4$  is considered. As stated in [32], the inter-element spacing of the AVS array is set to one wavelength to decorrelate noise across adjacent sensors, ensuring the covariance matrix approximates Gaussian white noise. In addition, in each Monte Carlo simulation experiment, the TVAD  $\{\beta_{mz}\}_{m=1}^M$  in the  $z$ th STP is randomly sampled from a normal distribution, with the mean  $\mu$  and the variance  $\rho^2$  specified for that particular experiment. The far-field narrowband source has equal power and uncorrelated components, represented by a complex exponential signal at center frequency  $f = 700$  Hz, sampled at  $f_s = 32$  KHz. Without any specific explanation, following [36], the regularization parameters  $\lambda_c$  and  $\lambda_s$  are both configured as 0.625 in the proposed method. Based on the analytical guidance and performance evaluation presented in [41], the user-defined parameter  $q$  is set to 0.5. The root mean square error (RMSE) for DOA estimation serves as one of the key evaluation metrics and can be formulated as

$$RMSE = \sqrt{\frac{1}{KU} \sum_{u=1}^U \sum_{k=1}^K (\hat{\theta}_{ku} - \theta_k)}, \quad (68)$$

where  $U = 5000$  is the number of Monte Carlo trials, and  $\hat{\theta}_{ku}$  represents the estimated result of  $\theta_k$  by in  $u$ th test. All numerical simulations were performed using MATLAB R2022a on a Windows 10 workstation equipped with a 2.50 GHz dual-core processor. In addition, the noise received by the AVS array, under the assumption of spherical isotropy, is presumed to be characterized by a noise covariance matrix that encompasses three distinct scenarios:

(1) The covariance matrix with the uniform noise in the  $z$ th STP is denoted as

$$\mathbf{Q}_z = \sigma_z^2 \mathbf{E}_{3M}, \quad (69)$$

where  $\sigma_z^2$  is the noise variance at each sensor.

(2) According to [21], [32], the covariance matrix with the ambient noise is generated as

$$\mathbf{Q}_z = diag\{1, 0.5, 0.5, 1, 0.5, 0.5, 1, 0.5, 0.5, 1, 0.5, 0.5\}. \quad (70)$$

(3) The covariance matrix with the non-uniform noise in the  $z$ th STP is generated according to [30], [33], where

$$\mathbf{Q}_z = diag\{\mathbf{q}_z\}, \quad (71)$$

where  $\mathbf{q}_z = P_{\min} + (P_{\max} - P_{\min}) \times rand(3M, 1)$  represents the  $3M \times 1$ -dimension vector of noise power in the  $z$ th STP with  $P_{\min}$  and  $P_{\max}$  being used to represent the upper and lower bounds of noise power, respectively, and  $rand(3M, 1)$  being a random vector, comprises elements that are uniformly distributed across a specified interval (0, 1).

As stated in [26], [30], [42], the SNR is defined as

$$SNR = \frac{\sigma_s^2}{3M} \sum_{l=1}^{3M} \frac{1}{\sigma_l^2}, \quad (72)$$

where  $\sigma_s^2$  represents the signal power, and  $\sigma_l^2$  denote the noise variance of the  $l$ th sensor.

##### A. Analysis of the Effect of Iteration Times on the Performance of the Proposed Algorithm

We assume that two narrowband uncorrelated signals impinge onto the AVS array from directions  $\theta_1 = -14^\circ$  and  $\theta_2 = 31^\circ$ , where  $L = 2000$ ,  $Z = 4$ ,  $\mu = 20$ ,  $\rho^2 = 3$ ,  $P_{\min} = 1$  and  $P_{\max} = 20$ , and the SNR is set to 3 dB. In Figs. 2(a) and 2(b), we present the curves of iteration error (IE) and CPU running time with different iteration times for three different scenarios:  $M = 3$ ,  $M = 5$ ,  $M = 7$ , where the IE is defined as  $\|\hat{\mathbf{P}}^{(j+1)} - \hat{\mathbf{P}}^{(j)}\|_2^2$ . It can be seen from Fig. 2(a) that the fastest error reduction was achieved when  $M = 7$ , and the lowest IE value was maintained in all iterations. Although there is a decreasing trend in error under different numbers of AVSs, excellent convergence is observed when  $M = 7$ , especially after 15 iterations, where the error drops below the errors of  $M = 5$  and  $M = 3$ . It is worth noting that compared to its curve, the convergence speed of  $M = 3$  is the slowest, and its error stabilizes at a higher value. This indicates that increasing the number of AVS can improve the stability and accuracy of the proposed algorithm. However, it may increase computational costs. This result can be clearly shown in Fig. 2(b), from which it is obvious that the proposed method requires the least amount of CPU time when  $M = 3$ . It shows moderate efficiency when  $M = 5$ , while  $M = 7$  has the highest computational efficiency. It is worth noting that as the iteration progresses, the CPU time at different numbers of elements shows an upward trend, indicating that regardless of the  $M$  value, the computational cost will increase with the continuous iteration. However, the difference in running time between different numbers of elements indicates that the choice of  $M$  will significantly affect the computational requirements. In the following simulation, we set  $M = 4$ . In our proposed method, the termination condition for iteration is  $T_{\max} = 25$  or  $\ell = 10^{-3}$ .

##### B. The Convergence Speed of the Proposed Method with Regularization Parameters

Fig. 3 shows the curves of iteration times and IE for six regularization parameter scenarios and the simulation parameters are the same as the previous experiment. From Fig. 3, we can see that as the number of iterations increases, the IE gradually decreases and tends to stabilize under different regularization parameters. The difference is that the convergence speed varies significantly depending on the regularization parameters. It is significant that the convergence speed of the proposed method is the fastest and the IE is the lowest when  $\lambda_c = \lambda_s = 0.6$ . Therefore, based on the statement in [36], the regularization parameters  $\lambda_c$  and  $\lambda_s$  are both configured as 0.625 in the our proposed method.

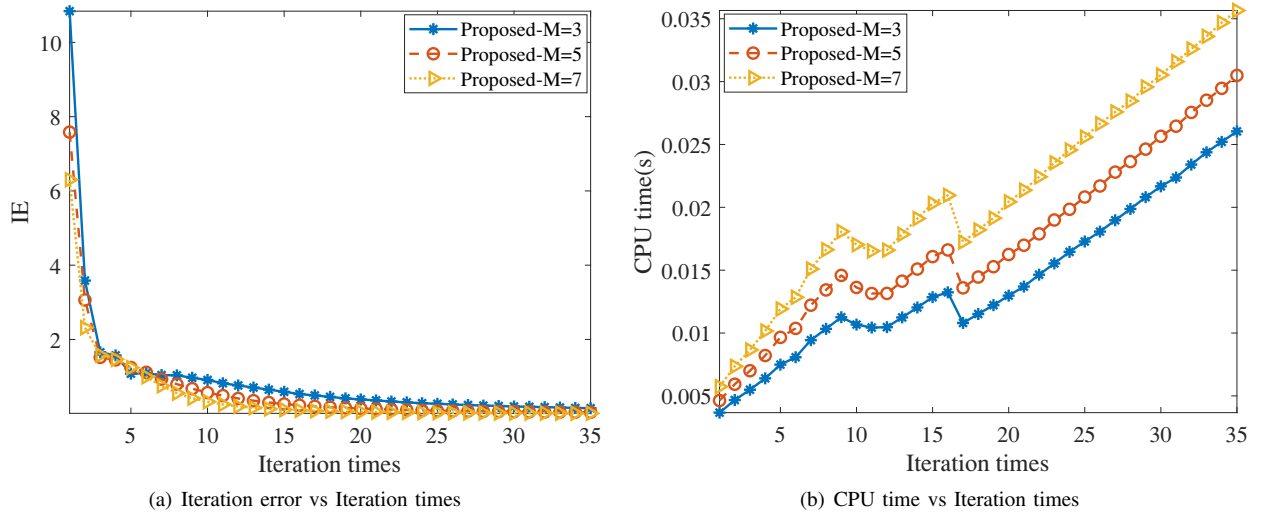


Fig. 2. The performance of the proposed method based on iteration times for two targets at  $(-14^\circ, 31^\circ)$  having  $\mu = 20$ ,  $\rho^2 = 4$ ,  $L = 2000$ ,  $Z = 4$ ,  $P_{\min} = 1$ ,  $P_{\max} = 20$  and SNR = 3 dB.

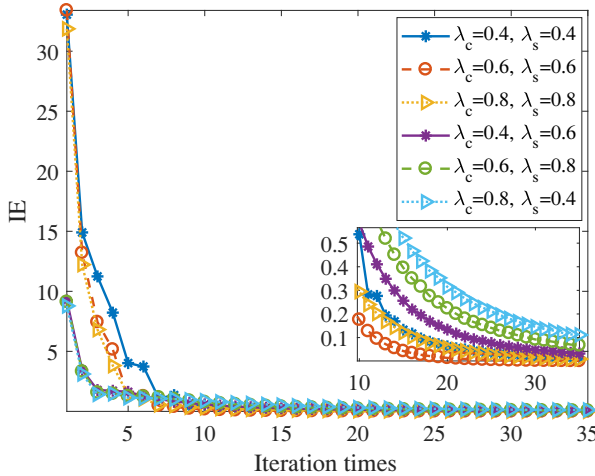


Fig. 3. The performance of the proposed method based on iteration times for two targets at  $(-14^\circ, 31^\circ)$  having  $\mu = 20$ ,  $\rho^2 = 4$ ,  $L = 2000$ ,  $Z = 4$ ,  $P_{\min} = 1$ ,  $P_{\max} = 20$ , and SNR = 3 dB.

### C. RMSE Varies with SNR under Different Noise Covariance Matrices and without Axial Deviation

We compared several RMSE variations with SNR under different noise covariance matrices without axial deviation, where the SNR varying between -10 dB and 15 dB, and the parameters are set to  $L = 2000$ ,  $Z = 4$ ,  $\mu = 0$ ,  $\rho^2 = 0$ . A comparative analysis of the RMSE between the proposed method and existing approaches is presented in Figs. 4(a), 4(b), and 4(c), respectively, for scenarios involving uniform noise, ambient noise, and non-uniform noise. Fig. 4(a) illustrates a notable deterioration in the DOA estimation performance of MUSIC, ASMUSIC, and ANEMUSIC methods, as compared to IAA, CMFF, and our proposed approach, particularly in low SNR regions. This degradation stems from the inability of eigen-decomposition of the array covariance matrix to accurately discern between signal and noise subspaces, leading to substantial DOA estimation errors. While

CMFF excels in low SNR scenarios, its performance lags behind other methods at higher SNRs. As SNR increases, the RMSE of all methods decreases, converging for MUSIC, ANEMUSIC, and our method above 12.5 dB SNR. Notably, our proposed method significantly outperforms others at SNRs below 12.5 dB. Under ambient noise, Fig. 4(b) reveals that the DOA estimation error of MUSIC remains relatively high across all SNR ranges. ASMUSIC fails to perform adequately when SNR falls below 2.5 dB. For SNRs exceeding 10 dB, IAA, ASMUSIC, ANEMUSIC, CMFF, and our method exhibit comparable DOA estimation performance, yet our method stands out with superior accuracy below 10 dB SNR. Comparing Figs. 4(a) and 4(b), the introduction of non-uniform noise adversely affects the performance of all methods, as seen in Fig. 4(c). Despite this degradation, our proposed method maintains the lowest RMSE, showcasing its robustness in DOA estimation amidst uniform, ambient, and non-uniform noise conditions.

### D. RMSE Varies with SNR under Different Noise Covariance Matrices and Axial Deviation

To delve deeper into the performance capabilities of our proposed method for an AVS array with axial deviation, we maintain all previously mentioned settings constant, except that  $\mu = 20$  and  $\rho^2 = 4$ . The plots in Figs. 5(a), 5(b), and 5(c) depict the RMSE of DOA estimation versus SNR under uniform noise, ambient noise, and non-uniform noise conditions. As evident in plot 5(a), the RMSE of MUSIC, IAA, ASMUSIC, and ANEMUSIC algorithms decreases with increasing SNR in the context of homogeneous interference and axial misalignment, since these methods overlook the impact of longitudinal distortion that varies over time for the computation of DOA. While both CMFF and the proposed method exhibit excellent performance across the entire SNR range, the proposed method's RMSE curve closely aligns with the CRLB, indicating superior DOA estimation accuracy. In Fig. 5(b), despite ASMUSIC and ANEMUSIC considering

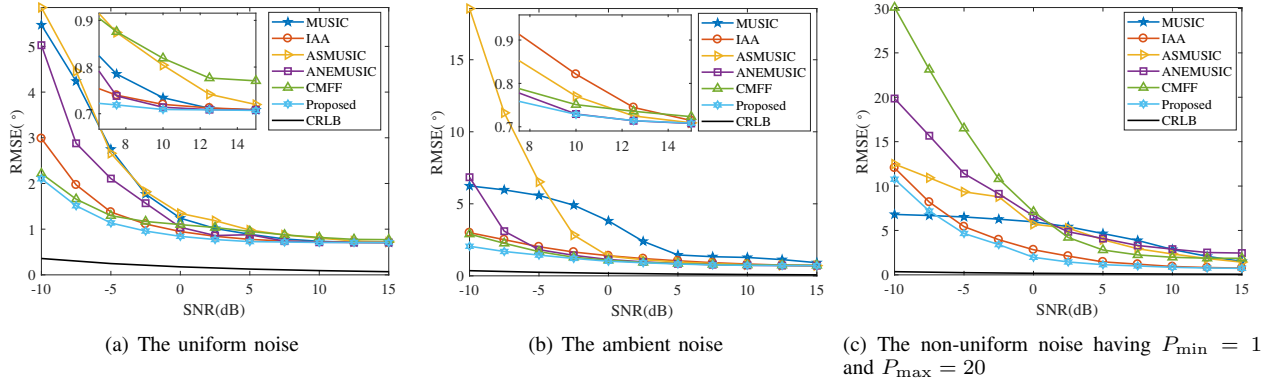


Fig. 4. Plot of RMSE against SNR for two targets at  $(-14^\circ, 31^\circ)$  having  $\rho^2 = 0$ ,  $L = 2000$ ,  $Z = 4$ , and  $\mu = 0$ .

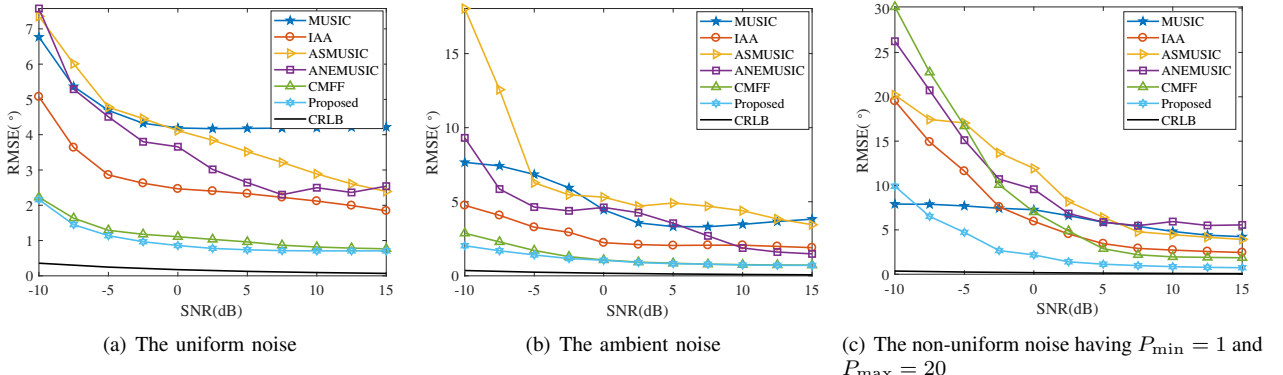


Fig. 5. Plot of RMSE against SNR for two targets at  $(-14^\circ, 31^\circ)$  having  $\rho^2 = 4$ ,  $L = 2000$ ,  $Z = 4$ , and  $\mu = 20$ .

ambient noise, their failure to account for TVAD leads to a significant decline in DOA prediction analysis. For SNRs higher than  $-2.5$  dB, the RMSE curves of CMFF and the proposed method align closely. However, for SNR below  $-2.5$  dB, the RMSE of the proposed method is lower. Fig. 5(c) presents the RMSE of all compared methods under non-uniform noise. Notably, even at high SNRs, their RMSE curves remain substantially distant from the CRLB. For SNR exceeding  $-7.5$  dB, the RMSE plot of the suggested algorithm consistently maintains the closest proximity to the CRLB. By comparing Figs. 5(a), 5(b), and 5(c), it is obvious that the proposed method consistently excels across all noise conditions (uniform, ambient, non-uniform) by effectively addressing TVAD. Its RMSE closely follows the CRLB, particularly in low SNR regimes, confirming its superior DOA estimation capability for AVS arrays with axial deviation.

#### E. CPU Varies with SNR under Different Noise Covariance Matrices and Axial Deviation

Fig. 6 compares the CPU running time of several algorithms at different SNR levels for three different noise scenarios: the uniform noise, the ambient noise, and the non-uniform noise. From Fig. 6(a), we can find that the proposed method maintains the highest CPU time value across the entire SNR range. The MUSIC, ASMUSIC, and ANEMUSIC methods show the low computational cost, while CMFF and IAA exhibit moderate performance. It is worth noting that regardless

of how the SNR ratio changes, all algorithms exhibit relatively stable computational requirements, indicating that their computational complexity is largely independent of the input signal quality. Compared to the scenario with uniform noise, we can see from Figs. 6(b) and 6(c) that the CPU running time of several algorithms has increased under ambient noise and non-uniform noise. Under ambient noise, the traditional MUSIC method, ASMUSIC method, and ANEMUSIC method have relatively stable CPU running time throughout the entire SNR range, and the CPU running time is significantly smaller than the iterative IAA, CMFF, and the proposed methods. However, the CPU running time of the IAA, CMFF, and the proposed methods increase at high SNR compared to low SNR. In non-uniform noise environments, traditional MUSIC, ASMUSIC, and ANEMUSIC methods still maintain low CPU runtime. Although the IAA, CMFF, and proposed methods have relatively stable CPU running time across the entire SNR range, the CPU running time is still longer than traditional MUSIC, ASMUSIC, and ANEMUSIC methods, and the CPU running time of the proposed method is the longest.

#### F. RMSE Varies with the Mean $\mu$ under Different Noise Covariance Matrices

Next, we inspect the effect of the mean  $\mu$  on DOA estimates under uniform noise, ambient noise, and non-uniform noise. In this case, we set simulation parameters consistent with Fig. 5, except that the mean  $\mu$  varies from 5 to 45 and

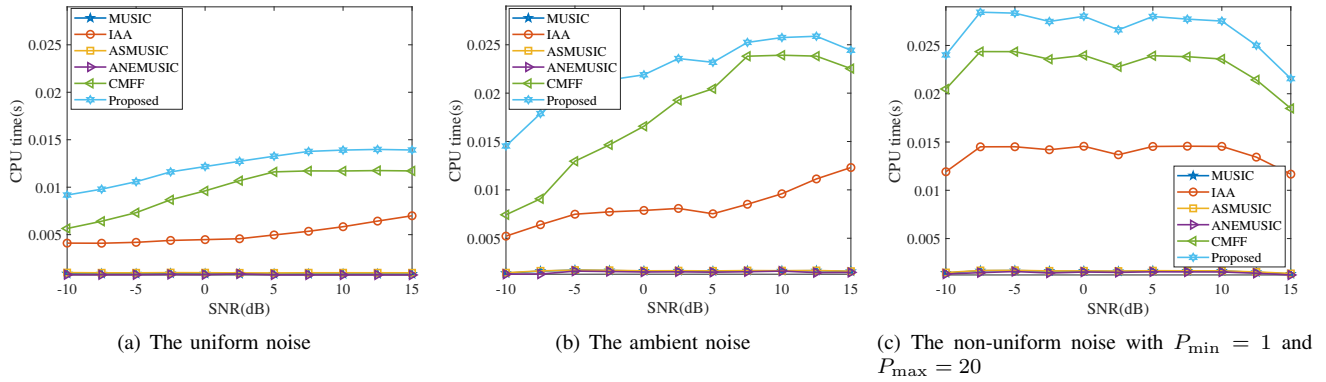


Fig. 6. Plot of CPU against SNR for two targets at  $(-14^\circ, 31^\circ)$  having  $\rho^2 = 4$ ,  $L = 2000$ ,  $Z = 4$ , and  $\mu = 20$ .

$\text{SNR} = 3$  dB. The RMSE of these approaches under conditions of uniform noise, ambient noise, and non-uniform noise is illustrated in Figs. 7(a), 7(b), and 7(c), correspondingly. In Figs. 7(a), 7(b), and 7(c), it is evident that the effectiveness of the MUSIC, IAA, ASMUSIC, and ANEMUSIC techniques noticeably diminishes when subjected to uniform noise, ambient noise, and non-uniform noise with a gradual increase in the mean  $\mu$ . Notably, the poorest performance is observed under non-uniform noise, followed by ambient noise. The proposed method outshines the CMFF method in accuracy, standing strong against all types of noise, be it uniform, ambient, or non-uniform, despite both methods being less affected by axial deviation. With a focus on both axial deviation and the varied effects of non-uniform noise, this is mainly attributed to the proposed method's potential. Furthermore, the RMSE of the proposed method remains relatively stable and unaffected by significant increases in the mean value ( $\mu$ ), regardless of whether the noise is uniform, ambient, or non-uniform. The consistency emphasizes the strength and effectiveness of the suggested DOA estimation approach. It should be noted that Figs. 7(a), 7(b), and 7(c) are all based on the assumption that each STP has the same mean value. Figs. 8(a), 8(b), and 8(c) show the simulation results with different mean values in each STP, where we set  $Z = 4$ , that is, the data collected by the AVS array is divided into four STPs, and the axial deviation of each STP has different mean values. To simplify the model, we assume that the mean value of the previous STP is 1 greater than that of the next STP, and the maximum value of the mean value in each STP is represented by  $\mu_{\max}$ . Other simulation parameters are consistent with Fig. 7. As can be seen from Figs. 8(a), 8(b), and 8(c), with the gradual increase of  $\mu_{\max}$ , the performance of different algorithms is deteriorated in the case of uniform noise, ambient noise, and non-uniform noise. In addition, compared with Figs. 7(a), 7(b), and 7(c), it can be seen that under the same noise environment conditions, the greater the average value in each STP, the worse the performance.

#### G. RMSE Varies with the Standard Variance $\rho$ under Different Noise Covariance Matrices

We also conducted performance testing of these methods for standard variance  $\rho$  under different noise covariance matrices,

where  $\rho$  varies from 0 to 40,  $\mu = 20$ , and other settings are the same as Fig. 7. From Figs. 9(a), 9(b), and 9(c), it can be seen that as the standard deviation  $\rho$  gradually increases, the performance of MUSIC, IAA, ASMUSIC, and ANEMUSIC methods deteriorates significantly under different noise covariance matrices, and their performance is the worst in non-uniform noise. By comparing Figs. 9(a) and 9(b), it can be seen that the ASMUSIC and ANEMUSIC methods, which consider the ambient noise, have failed to resist the ambient noise under the influence of axial deviation. This is mainly reflected in the fact that the RMSE under uniform noise is slightly smaller than their RMSE under ambient noise. While a slight discrepancy in RMSE is observed between the CMFF technique and our method in the presence of uniform and ambient noise, the proposed approach demonstrates notably superior RMSE performance over the CMFF method in situations where non-uniform noise is present. The robustness of our proposed DOA estimation method is highlighted by this observation, especially in handling non-uniform noise.

#### H. RMSE Exhibits Variability in Accordance with the Maximum Noise Power Constraint $P_{\max}$

Finally, we evaluated the RMSE of the proposed approach using varying upper bounds of noise power  $P_{\max}$  under conditions both with and without axial deviation. The simulation parameters are kept consistent with Fig. 5, except for the variation of the upper bound of noise power  $P_{\max}$  ranging from 10 to 80, while maintaining  $\text{SNR} = 3$  dB. The RMSE of these comparison methods without axial deviation are shown in Fig. 10(a) and the RMSE of these comparison methods with axial deviation are given in Fig. 10(b). As evident from Fig. 10(a), the MUSIC, ASMUSIC, ANEMUSIC, and CMFF methods overlooked the impact of unequal noise power across array elements, leading to suboptimal DOA estimation. Although the IMLSE method considers the influence of non-uniform noise, it does not take into account the impact of axial deviation, which deteriorates its estimation performance. Notably, the CMFF method's DOA estimation accuracy was most sensitive to the upper bound of noise power  $P_{\max}$ . Both the IAA method and the proposed method address the impacts of non-uniform noise; however, the proposed method demonstrates significantly greater accuracy in estimating DOA

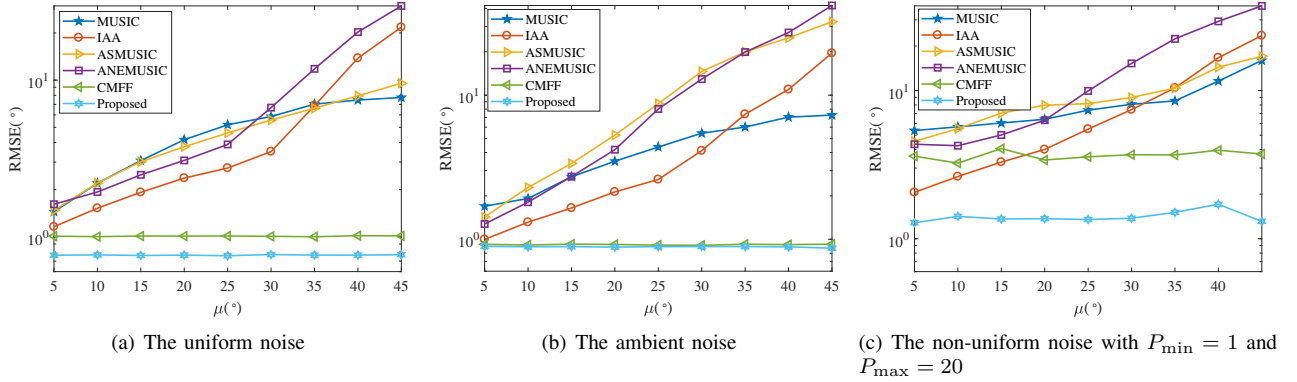


Fig. 7. Plot of RMSE against  $\mu$  for two targets at  $(-14^\circ, 31^\circ)$  having  $\rho^2 = 4$ ,  $L = 2000$ ,  $Z = 4$ , and SNR = 3 dB.

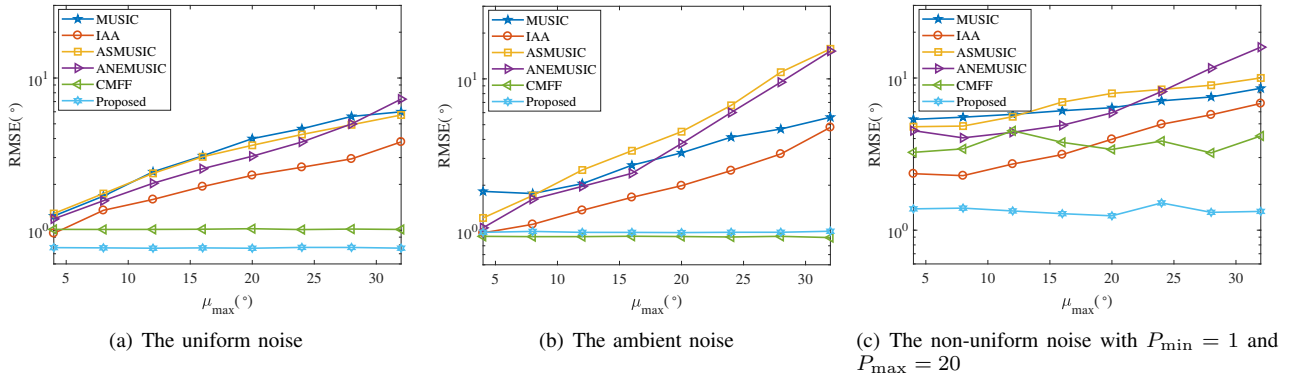


Fig. 8. Plot of RMSE against  $\mu$  for two targets at  $(-14^\circ, 31^\circ)$  having  $\rho^2 = 4$ ,  $L = 2000$ ,  $Z = 4$ , and SNR = 3 dB.

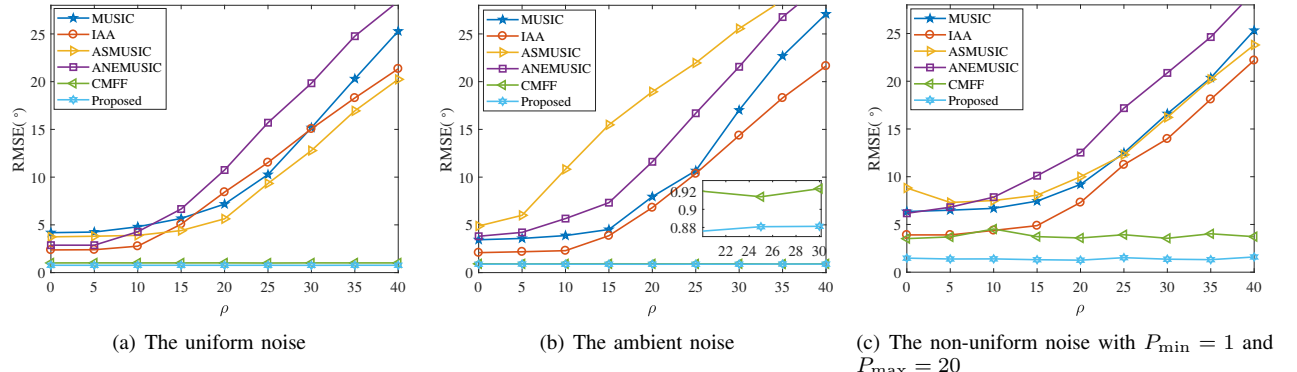


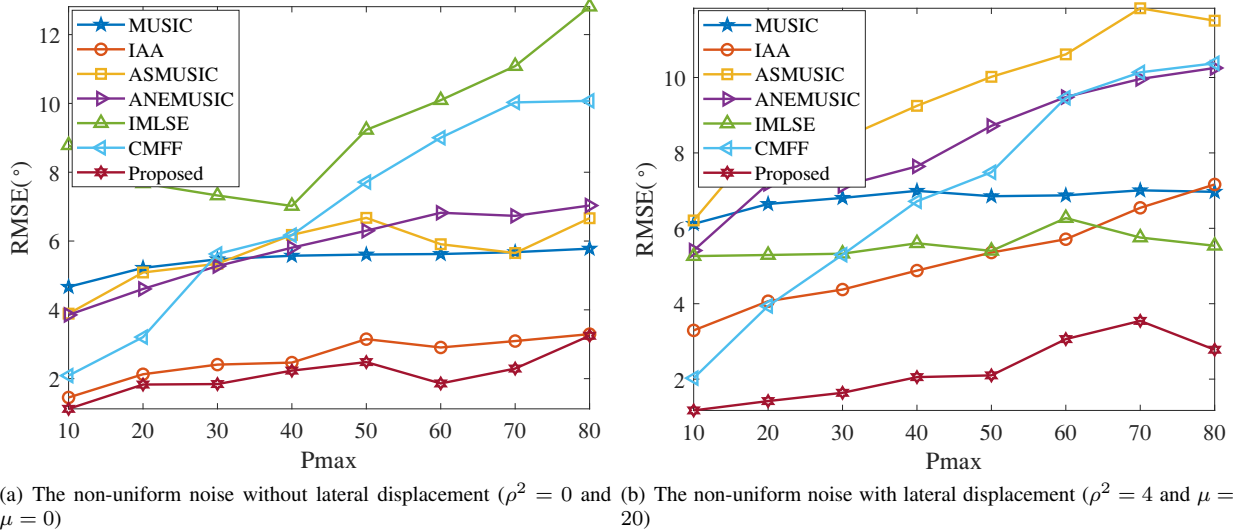
Fig. 9. Plot of RMSE against  $\rho$  for two targets at  $(-14^\circ, 31^\circ)$  having  $\mu = 20$ ,  $L = 2000$ ,  $Z = 4$ , and SNR = 3 dB.

when compared to the IAA method. From Fig. 10(b), the proposed method demonstrates superior estimation accuracy, achieving the lowest RMSE values across the entire  $P_{\max}$  range. It is evident that the DOA estimation accuracy of the MUSIC, ASMUSIC, ANEMUSIC, IMLSE and IAA algorithms is notably hindered by both non-uniform noise and axial misalignment. In contrast to their performance without axial deviation (shown in Fig. 10(a)), the presence of axial deviation adversely affects their accuracy. However, the CMFF method displays a moderate resistance to axial deviation, as indicated by its reduced RMSE compared to Fig. 10(a). The proposed method, which considers both axial deviation and non-uniform noise, demonstrates the best overall estimation

performance across the full range of  $P_{\max}$ . A comparison of Figs. 10(a) and 10(b) reveals that the proposed method demonstrates superior and consistent DOA estimation accuracy across varying noise power levels compared to existing methods, with particularly strong performance advantages in moderate power ranges. This suggests it is more robust and reliable for practical applications where the noise power levels may vary.

## V. CONCLUSION

The article introduces a two-step least squares fitting (TSLSF) method to tackle the direction of arrival (DOA)

Fig. 10. RMSE versus WNPR for two sources at  $(-14^\circ, 31^\circ)$  with SNR = 3 dB,  $L = 2000$ ,  $Z = 4$ .

estimation challenge employing the AVS array with TVAD amidst non-uniform noise condition. In the proposed TSLSF method, by introducing axial deviation parameters into datasets of different STP, we established the model of AVS array under TVAD. Then, the cost function for the TVAD matrix was defined, and then an analytical expression for it was obtained. According to the predicted outcomes of the axial deviation matrix, the focusing technology is used to transform datasets with TVAD from different STPs into the reference STP. Moreover, we formulated a novel AVS array manifold matrix to process the noise vectors of every link in the AVS array, and formulated the cost function by fitting the interference and noise variance function to estimate sparse signals and noise vector. Simulation experiments have demonstrated the potential and resilience of suggested technique within the AVS array utilizing TVAD in the presence of varying levels of noise.

## REFERENCES

- [1] A. Nehorai and E. Paldi, "Acoustic vector-sensor array processing," *IEEE Trans. Signal Process.*, vol. 42, no. 9, pp. 2481–2491, 1994.
- [2] M. Hawkes and A. Nehorai, "Acoustic vector-sensor beamforming and capon direction estimation," *IEEE Trans. Signal Process.*, vol. 46, no. 9, pp. 2291–2304, 1998.
- [3] A. M. Thode *et al.*, "Acoustic vector sensor beamforming reduces masking from underwater industrial noise during passive monitoring," *J. Acoust. Soc. America*, vol. 139, no. 4, pp. EL105–EL111, 2016.
- [4] A. Gunes and M. B. Guldogan, "Joint underwater target detection and tracking with the bernoulli filter using an acoustic vector sensor," *Digital Signal Process.*, vol. 48, pp. 246–258, 2016.
- [5] F. A. Bozzi and S. M. Jesus, "Joint vector sensor beam steering and passive time reversal for underwater acoustic communications," *IEEE Access*, vol. 10, pp. 66 952–66 960, 2022.
- [6] K. Raghukumar, G. Chang, F. Spada, and C. Jones, "A vector sensor-based acoustic characterization system for marine renewable energy," *J. Marine Sci. Eng.*, vol. 8, no. 3, p. 187, 2020.
- [7] M. Rawat, B. Lall, and S. Srirangarajan, "Statistical modeling and performance analysis of cooperative communication in frequency-selective underwater acoustic channel using vector sensor," *IEEE Sensors J.*, vol. 21, no. 6, pp. 7367–7379, 2021.
- [8] Y. Liu *et al.*, "Research on DOA estimation method of single mems vector hydrophone based on pulse signal," *Sensors and Actuators A: Physical*, vol. 346, p. 113859, 2022.
- [9] R. H. Roy III and T. Kailath, "Esprit—estimation of signal parameters via rotational invariance techniques," *Opt. Eng.*, vol. 29, no. 4, pp. 296–313, 1990.
- [10] F. Li, H. Liu, and R. J. Vaccaro, "Performance analysis for DOA estimation algorithms: Unification, simplification, and observations," *IEEE Trans. Aerosp. Electron. Syst.*, vol. 29, no. 4, pp. 1170–1184, 1993.
- [11] D. Malioutov, M. Cetin, and A. S. Willsky, "A sparse signal reconstruction perspective for source localization with sensor arrays," *IEEE Trans. Signal Process.*, vol. 53, no. 8, pp. 3010–3022, 2005.
- [12] T. Yardibi, J. Li, P. Stoica, M. Xue, and A. B. Bagheroer, "Source localization and sensing: A nonparametric iterative adaptive approach based on weighted least squares," *IEEE Trans. Aerosp. Electron. Syst.*, vol. 46, no. 1, pp. 425–443, 2010.
- [13] Y.-X. Zou, B. Li, and C. H. Ritz, "Multi-source DOA estimation using an acoustic vector sensor array under a spatial sparse representation framework," *Circuits, Syst., Signal Process.*, vol. 35, pp. 993–1020, 2016.
- [14] D. Mao *et al.*, "Target fast reconstruction of real aperture radar using data extrapolation-based parallel iterative adaptive approach," *IEEE J. Sel. Topics Appl. Earth Observ. Remote Sens.*, vol. 14, pp. 2258–2269, 2021.
- [15] Z. Yao and R. Guo, "High accuracy ESPRIT without left-right ambiguity using an acoustic vector sensor array," in *Proc. IEEE/OES COA*, 2016.
- [16] A. Zhao, L. Ma, J. Hui, C. Zeng, and X. Bi, "Open-lake experimental investigation of azimuth angle estimation using a single acoustic vector sensor," *J. Sensors*, vol. 2018, 2018.
- [17] S. Liu, J. Zhao, Y. Zhang, and D. Wu, "2D DOA estimation algorithm by nested acoustic vector-sensor array," *Circuits, Syst., Signal Process.*, pp. 1–16, 2022.
- [18] S. Shi, Y. Li, D. Yang, A. Liu, and J. Shi, "Sparse representation based direction-of-arrival estimation using circular acoustic vector sensor arrays," *Digital Signal Process.*, vol. 99, p. 102675, 2020.
- [19] W. Wang and W.-J. Tan, "Alternating iterative adaptive approach for DOA estimation via acoustic vector sensor array under directivity bias," *IEEE Commun. Lett.*, vol. 24, no. 9, pp. 1944–1948, 2020.
- [20] S. Shi, Y. Li, D. Yang, A. Liu, and Z. Zhu, "DOA estimation of coherent signals based on the sparse representation for acoustic vector-sensor arrays," *Circuits, Syst., Signal Process.*, vol. 39, pp. 3553–3573, 2020.
- [21] A. Liu, D. Yang, S. Shi, Z. Zhu, and Y. Li, "Augmented subspace music method for DOA estimation using acoustic vector sensor array," *IET Radar, Sonar & Navigation*, vol. 13, no. 6, pp. 969–975, 2019.
- [22] A. Liu, S. Shi, and X. Wang, "Robust DOA estimation method for underwater acoustic vector sensor array in presence of ambient noise," *IEEE Trans. Geosci. Remote Sens.*, vol. 61, p. 4206014, 2023.
- [23] M. Pesavento and A. B. Gershman, "Maximum-likelihood direction-of-arrival estimation in the presence of unknown nonuniform noise," *IEEE Trans. Signal Process.*, vol. 49, no. 7, pp. 1310–1324, 2001.
- [24] D. Madurasinghe, "A new DOA estimator in nonuniform noise," *IEEE Signal Process. Lett.*, vol. 12, no. 4, pp. 337–339, 2005.

- [25] C. E. Chen, F. Lorenzelli, R. E. Hudson, and K. Yao, "Stochastic maximum-likelihood DOA estimation in the presence of unknown nonuniform noise," *IEEE Trans. Signal Process.*, vol. 56, no. 7, pp. 3038–3044, 2008.
- [26] B. Liao, S.-C. Chan, L. Huang, and C. Guo, "Iterative methods for subspace and DOA estimation in nonuniform noise," *IEEE Trans. Signal Process.*, vol. 64, no. 12, pp. 3008–3020, 2016.
- [27] J. Cong, X. Wang, X. Lan, and W. Liu, "A generalized noise reconstruction approach for robust DOA estimation," *IEEE Trans. Radar Syst.*, 2023.
- [28] M. Wang, Z. Zhu, F. Chen, and H. Wang, "Coordinate descent method for avs linear array DOA estimation in non-uniform noise," *IEEE Sensors J.*, vol. 24, no. 7, pp. 10 742–10 754, 2024.
- [29] W. Shi, X. Li, W. Wang, W. Tan, and H. Li, "Direction of arrival estimation for a non-ideal acoustic vector hydrophone array," *Appl. Acoust.*, vol. 190, p. 108636, 2022.
- [30] S. Shi *et al.*, "Eigenstructure methods for DOA estimation of circular acoustic vector sensor array with axial angle bias in nonuniform noise," *Digital Signal Process.*, vol. 147, p. 104404, 2024.
- [31] W. Wang, X. Li, Z. Liu, W. Shi, and H. Li, "Direction finding method via acoustic vector sensor array with fluctuating misorientation," *Appl. Acoust.*, vol. 211, p. 109469, 2023.
- [32] M. Hawkes and A. Nehorai, "Acoustic vector-sensor correlations in ambient noise," *IEEE J. Ocean. Eng.*, vol. 26, no. 3, pp. 337–347, 2001.
- [33] W. Wang, Q. Zhang, W. Shi, W. Tan, and L. Mao, "Off-grid DOA estimation based on alternating iterative weighted least squares for acoustic vector hydrophone array," *Circuits, Syst., Signal Process.*, vol. 39, pp. 4650–4680, 2020.
- [34] M. A. T. Figueiredo, J. M. Bioucas-Dias, and R. D. Nowak, "Majorization-minimization algorithms for wavelet-based image restoration," *IEEE Trans. Image Process.*, vol. 16, no. 12, pp. 2980–2991, 2007.
- [35] K. Han and A. Nehorai, "Improved source number detection and direction estimation with nested arrays and ULAs using jackknifing," *IEEE Trans. Signal Process.*, vol. 61, no. 23, pp. 6118–6128, 2013.
- [36] X. Wu, W.-P. Zhu, J. Yan, and Z. Zhang, "Two sparse-based methods for off-grid direction-of-arrival estimation," *Signal Process.*, vol. 142, pp. 87–95, 2018.
- [37] X. Tan, W. Roberts, J. Li, and P. Stoica, "Sparse learning via iterative minimization with application to MIMO radar imaging," *IEEE Trans. Signal Process.*, vol. 59, no. 3, pp. 1088–1101, 2010.
- [38] H. Abeida, Q. Zhang, J. Li, and N. Merabtine, "Iterative sparse asymptotic minimum variance based approaches for array processing," *IEEE Trans. Signal Process.*, vol. 61, no. 4, pp. 933–944, 2012.
- [39] S. Najeem, K. Kiran, A. Malarkodi, and G. Latha, "Open lake experiment for direction of arrival estimation using acoustic vector sensor array," *Appl. Acoust.*, vol. 119, pp. 94–100, 2017.
- [40] P. K. Tam and K. T. Wong, "Cramér-rao bounds for direction finding by an acoustic vector sensor under nonideal gain-phase responses, noncollocation, or nonorthogonal orientation," *IEEE Sensors J.*, vol. 9, no. 8, pp. 969–982, 2009.
- [41] Z. Xu, X. Chang, F. Xu, and H. Zhang, " $l_{1/2}$  regularization: A thresholding representation theory and a fast solver," *IEEE Trans. Neural Netw. Learn. Syst.*, vol. 23, no. 7, pp. 1013–1027, 2012.
- [42] F. Shafee, A. Mahmoudi, and B. Dumitrescu, "Linear prediction-based DO estimator in non-uniform noise," *Circuits, Syst., Signal Process.*, vol. 40, no. 5, pp. 2494–2506, 2021.



**Affaq Qamar** is an accomplished researcher and educator specializing in modelling and optimization of embedded systems, and modern technologies in smart grids. With a Ph.D. in Electrical Engineering from Politecnico di Torino, Italy, his work focuses on sustainable energy solutions and advanced technological innovations. Dr. Affaq has contributed significantly to areas such as hybrid microgrid systems, low-energy smart buildings, and energy-efficient architectures. His research is widely published, showcasing his expertise in addressing modern challenges in energy and embedded systems.



**Linya Ma** obtained the B.E. degree in Physics and Electronic Information Engineering from Zhoukou Normal University in Zhoukou, China in 2023. Currently, she is pursuing a Master's degree at Henan Polytechnic University in Jiaozuo, China. Her research interests include array signal processing and performance analysis, parameter estimation, and convex optimization.



**Hui Li** received the B.Sc. degree in Communication Engineering from the School of Information Engineering, in 1999, and the M.Sc. degree in Communication and Information System and the Ph.D. degree in Information and Communication Engineering from the Nanjing University of Science and Technology, in 2004 and 2008, respectively. He was a Visiting Scholar with Charles Darwin University, Australia, in 2013, and North Carolina Agricultural and Technical State University, in 2014. He is currently a Professor with the School of Physics and Electronic Information Engineering, Henan Polytechnic University, Jiaozuo China. His research interests include wireless communications and intelligent signal processing.



**Zhiqiang Liu** received the B.Sc. degree in Material Forming and Control Engineering from Jiaozuo Institute of Technology, China in 2003. He received the M.Sc. degree in Management Science and Engineering from Hebei University of Engineering, China in 2006. He received the Ph.D. degree in Security System from People's Public Security University of China, China in 2020. Currently, he is an Instructor in the College of Computer Science and Technology, Henan Polytechnic University, China. His research interests include computer vision and image processing.



**Wentao Shi** (Senior Member, IEEE) received the B.Sc. degree in Electrical Engineering, and the M.S. and Ph.D. degrees in Information and Communication Engineering from Northwestern Polytechnical University in 2007, 2010, and 2012, respectively. From 2010 to 2011, he was a Visiting Scholar with the Department of Electrical and Computer Engineering, University of Minnesota. He is currently an Professor with the Ocean Institute, Northwestern Polytechnical University, Taicang China. His research interests are array signal processing and MIMO array signal processing.



**Weidong Wang** received the B.Sc. degree from the College of Computer and Information Engineering, Nanyang Institute of Technology, Nanyang, China, in 2014, and the M.S. degree from the School of Information Science and Engineering, Yunnan University, Kunming, China, in 2017, and the Ph.D. degree from the Armament Science and Technology, Northwestern Polytechnical University, Xi'an, China, in 2020. He has been to Concordia University in Canada for joint doctoral training during his PhD. He is currently a Lecturer with the School of Physics and Electronic Information Engineering, Henan Polytechnic University, Jiaozuo China. His research interests include array signal processing, parameter estimation, sparse signal representation, and convex optimization.



**Wasiq Ali** received the B.S. degree in Electronics Engineering from COMSATS University Islamabad, Abbottabad, Pakistan, in 2012, the M.S. degree in Electrical Engineering (Wireless Communication) from COMSATS University Islamabad, Attock, Pakistan, in 2015, and the Ph.D. degree in Underwater Acoustic Signal Processing from Northwestern Polytechnical University, Xi'an, China, in 2021. He is currently an Associate Professor with the College of Underwater Acoustic Engineering, Harbin Engineering University, Harbin, China. He also served as an Assistant Professor with the Department of Electrical and Computer Engineering, COMSATS University Islamabad, Attock Campus, Pakistan. Dr. Ali has authored more than 38 journal and conference papers. His current research interests include underwater acoustic signal processing, passive target tracking, direction-of-arrival estimation, and neural network-based intelligent computing techniques for ocean engineering applications.



**Sheeraz Akram** received the Master of Science degree in Computer Science from Lahore University of Management Sciences (LUMS), Lahore, Pakistan, and the Ph.D. degree in Software Engineering from the National University of Sciences and Technology (NUST), Islamabad, Pakistan. He completed his Postdoctoral research training with the University of Pittsburgh, worked on a project funded through grant U01 HL137159. He is currently an Associate Professor at Information Systems Department, College of Computer and Information Sciences, Imam Mohammad Ibn Saud Islamic University (IMSIU), Riyadh, Saudi Arabia. He actively leads and coordinates research activities with the Intelligent Data Visual Computing Research (IDVCR). He is a trained STEM professional from the University of Pittsburgh, USA.